Bosons in one-dimensional incommensurate superlattices

Tommaso Roscilde
Max-Planck-Institut für Quantenoptik, Hans-Kopfermann-strasse 1, 85748 Garching, Germany
(Received 21 December 2007; revised manuscript received 28 February 2008; published 9 June 2008; publisher error corrected 13 June 2008)

We investigate numerically the zero-temperature physics of the one-dimensional Bose-Hubbard model in an incommensurate cosine potential, recently realized in experiments with cold bosons in optical superlattices [L. Fallani *et al.*, Phys. Rev. Lett. **98**, 130404 (2007)]. An incommensurate cosine potential has intermediate properties between a truly periodic and a fully random potential, displaying a characteristic length scale (the quasiperiod) which is shown to set a finite lower bound to the excitation energy of the system at special incommensurate fillings. This leads to the emergence of gapped incommensurate band-insulator (IBI) phases along with gapless Bose-glass (BG) phases for strong quasiperiodic potential for both hard-core and soft-core bosons. Enriching the spatial features of the potential by the addition of a second incommensurate component appears to remove the IBI regions, stabilizing a continuous BG phase over an extended parameter range. Moreover, we discuss the validity of the local-density approximation in the presence of a parabolic trap, clarifying the notion of a *local* BG phase in a trapped system; we investigate the behavior of first- and second-order coherence upon increasing the strength of the quasiperiodic potential; and we discuss the *ab initio* derivation of the Bose-Hubbard Hamiltonian with quasiperiodic potential starting from the microscopic Hamiltonian of bosons in an incommensurate superlattice.

DOI: 10.1103/PhysRevA.77.063605 PACS number(s): 03.75.Lm, 71.23.Ft, 68.65.Cd, 72.15.Rn

I. INTRODUCTION

Localization effects in random potentials represent a striking manifestation of the wavelike nature of quantum particles, and they are particularly pronounced in dimensions less than 3, where, in the absence of an interaction, the suppression of transport due to disorder occurs at all energy scales [1,2]. A particularly intriguing aspect of localization phenomena is their subtle interplay with particle-particle interactions. In the following we will limit our discussion to *bosons*. The screening effect of weak interactions can lead to a transition from a localized (Anderson) insulator to a superfluid—namely, to the persistence of superfluidity in a disordered potential [3,4]. Systems on a commensurately filled lattice without disorder exhibit a gapped Mott-insulating (MI) phase for strong interactions, competing with a superfluid (SF) phase as the interaction is reduced; in the presence of disorder, the gapless *Bose-glass* (BG) insulator competes with the MI when the disorder strength becomes comparable with the Mott gap [4,5].

Recent experiments on trapped cold atoms have demonstrated the ability of loading an atomic Bose gas in a well-controlled disordered potential [6–11]. In particular, the regime of strong repulsion in a strong *pseudodisordered* potential has been achieved by loading cold bosons in a deep one-dimensional *quasiperiodic* (QP) optical superlattice, formed by two standing waves with incommensurate wavelengths [10]. In the insulating phase of the system, Bragg spectroscopy reveals an excitation spectrum which strongly differs from that of a MI, showing that the QP potential introduces many new states in the spectral Mott gaps, caused by the strong repulsion. This feature indirectly suggests that the insulating phase measured in the experiments could be a BG; yet, direct experimental inspection in the low-energy spectrum, which is decisive to distinguish a BG insulator from a more conventional MI, is currently not available.

On the theoretical side, the study of tight-binding models in QP potentials has a long history [12–16] connected to the fundamental question of the fate of Anderson localization in quasirandom potentials. Although Bloch's theorem does not apply to QP potentials, for one-dimensional systems it was soon realized that the single-particle spectrum of the system is composed of bands made of either *all* extended or *all* localized states depending on the potential strength. Therefore, filling such a system with spinless fermions leads to the appearance of incommensurate band-insulator (IBI) phases alternating with metallic phases for a weak QP potential and with Anderson-insulating ones for a strong QP potential. Remarkably, the very same picture can be exactly recovered for *bosons* in the hard-core repulsive limit [17,18], with the following correspondence between fermionic and bosonic phases: "metallic" → "superfluid" and "Anderson insulator" → "Bose glass."

In this paper we provide a systematic study of one-dimensional bosons in a QP potential. We explicitly map out the phase diagram of the system in the hard-core limit through exact diagonalization, reconstructing the tight alternation of the SF, IBI, and BG phases upon changing the chemical potential. Making use of quantum Monte Carlo techniques, we can then move on to the *soft-core* case which is the most appropriate for the experiments [10]. There we find that a strong QP potential, equaling in strength the interparticle repulsion, completely removes the MI phase, leaving space for various insulating phases at fractional fillings: similarly to the hard-core case, slight changes of the model parameters (chemical potential and hopping amplitude) can drive the system from BG to IBI in a tight alternation. Therefore the pseudodisorder created by a single incommensurate potential component leads to a significantly different phase diagram than in the case of a truly random potential [19–21], where a continuous BG appears, becoming the only insulat-

 ©2008 The American Physical Society

ing phase for strong enough disorder. The fundamental differences between a truly random potential and a QP one are explained quantitatively within a generalized atomic-limit approximation, which captures how the statistics of spatial structures in the potential reflects itself in the spectral properties. On the basis of this observation, we extend the degrees of freedom of the QP potential beyond what has been so far explored in experiments [10], in search of the minimal setup which would lead to a similar behavior to the case of a truly random potential. We find that the addition of a further incommensurate component, leading to a two-color QP potential, causes the removal of the IBI phases and hence to the appearance of a BG persisting over an extended filling range.

Moreover, we discuss the behavior of the system in the presence of a parabolic trap, mimicking the experimental situation encountered in current optical-lattice setups. The local-density approximation (LDA), generally successful in the absence of a QP potential, is critically discussed in its presence. On the one hand, the density profile and local particle-number fluctuations are correctly predicted by the LDA; on the other hand, the identification of the local behavior in the trapped system with that of the bulk system at the same chemical potential does not generally hold, due to the severeness of the finite-size effects imposed by the trap in the presence of the QP potential. At the same time we show that a two-color QP potential can realize a uniform BG phase in the trap, on average over the fluctuations of the spatial phases of the potential components. Finally we make a closer connection to optical-lattice experiments by investigating the behavior of the currently accessible observables, which are shown to reveal the full evolution of phase and density correlations in the system upon changing the strength of the QP potential; and we discuss in details the *ab initio* derivation of the one-dimensional Bose-Hubbard Hamiltonian in the case of an incommensurate optical superlattice.

This paper is structured as follows. Section II introduces the Bose-Hubbard model in an incommensurate cosine potential and the numerical methods used in the paper; Sec. III discusses the phase diagram in the hard-core limit; the phase diagram of the soft-core model is then presented in Sec. IV; Sec. V discusses the emergence of the IBI in the presence of the QP potential; Sec. VI focuses on the local-density approximation in the trapped system; Sec. VII shows results for the experimental observables; and Sec. VIII presents the *ab initio* derivation of the Bose-Hubbard Hamiltonian. Summary and conclusions are presented in Sec. IX.

II. MODEL AND METHODS

We investigate the one-dimensional Bose-Hubbard model in an incommensurate cosine potential, with Hamiltonian

$$\mathcal{H}_0 = \sum_{i=1}^{L} \left\{ -J(b_i b_{i+1}^\dagger + \text{H.c.}) + \frac{U}{2} n_i(n_i - 1) + V_2 g(i;\alpha,\phi) n_i - \mu n_i \right\}, \quad (1)$$

with

$$g(i;\alpha,\phi) = \cos^2(\pi\alpha\ \ i + \phi) - \frac{1}{2} = \frac{\cos(2\pi\alpha\ \ i + 2\phi)}{2}, \quad (2)$$

where b_i and $b_i^\dagger$ are bosonic operators, J is the hopping amplitude, U is the on-site repulsion, V_2 is the strength of the QP potential, and μ is the chemical potential. The incommensuration parameter $0<\alpha<1$ is in principle an *irrational* number; making use of periodic boundary conditions, it is appropriate to take $\alpha = N_{\text{cycles}}/L$ (with noninteger L/N_{cycles}) so that the incommensurate cosine potential has a period exactly equal to the lattice size L.

The realization of the Bose-Hubbard model by loading cold bosons in the lowest band of an optical lattice [22] has been demonstrated by now in a large variety of experiments [23–25]. More recently Fallani *et al.* [10] have been able to add a QP potential to a one-dimensional optical lattice by application of a secondary standing wave, with an incommensurate wavelength λ_2 with respect to that (λ_1) of the primary lattice. If the intensity of the secondary wave is significantly weaker than that of the primary lattice, the main effect of the λ_2 lattice is to modulate the depth of the potential wells of the primary λ_1 lattice, as modeled by the V_2-term in Eq. (1) (see Sec. VIII for a thorough discussion of this point). We choose the representation of the incommensurate cosine potential as in Eq. (2) such that the potential strength V_2 reflects directly the intensity of a secondary standing wave at wavelength $\lambda_2 = \lambda_1/\alpha$: given that the first, dominant standing wave "discretizes" the space to points $x_i = (\lambda_1/2)\ \ i$, the secondary standing wave creates a potential on such points which is proportional to $\cos^2[(2\pi/\lambda_1)x_i + \phi] = \cos^2(\alpha\pi i + \phi)$ as in Eq. (2). The wavelength relation defines the incommensuration parameter, $\alpha = \lambda_1/\lambda_2 = 830.7/1076.8 = 0.771\ 37\ldots$. In the following we will use different rational approximants thereof ($\alpha \approx 97/126,\ \ 830/1076$).

A fundamental limit of the Bose-Hubbard model is the hard-core case $U \to \infty$, in which double occupancy is strictly forbidden and which has been experimentally demonstrated in Ref. [26]. In the hard-core limit the constraint of forbidden double occupancy can be directly incorporated in the operator algebra by introducing on-site anticommutation rules for the *hard-core-boson* operators, $\{a_i, a_i^\dagger\} = 1$ and $\{a_i^{(\dagger)}, a_i^{(\dagger)}\} = 0$, coexisting with ordinary bosonic commutation rules between different sites. Hard-core bosons can be exactly mapped onto spinless fermions f_i and $f_i^\dagger$ through the Jordan-Wigner transformation [27],

$$a_i^\dagger = f_i^\dagger \prod_{k=1}^{i-1} e^{-i\pi f_k^\dagger f_k}, \quad a_i = \prod_{k=1}^{i-1} e^{i\pi f_k^\dagger f_k} f_i, \quad (3)$$

so that the resulting Hamiltonian is that of free fermions in a potential:

$$\mathcal{H} = \sum_{i=1}^{L-1} [-J(f_i f_{i+1}^\dagger + \text{H.c.}) + V_2 g(i;\alpha,\phi) m_i - \mu m_i] - J(e^{i\theta} f_L f_1^\dagger + \text{H.c.}). \quad (4)$$

The boundary phase term resulting from the nonlocal nature of the Jordan-Wigner transformation reads $\theta = [(N+1) \pm 1]\pi$,

where N is the particle number and the sign + (−) applies to periodic (antiperiodic) boundary conditions.

Once reduced to spinless fermions, the hard-core boson problem is exactly solvable through simple single-particle diagonalization. In the following we will focus our attention on two fundamental quantities: namely, the *superfluid density*, estimated through the energy difference between periodic (+) and antiperiodic (−) boundary conditions,

$$\rho_s = \frac{L}{J\pi^2}(E^{(-)} - E^{(+)}), \tag{5}$$

and the compressibility $\kappa = dn/d\mu$, where $n = N/L$ is the particle density.

In the soft-core case of the original Hamiltonian (1) an exact solution is not available. In this case we make use of quantum Monte Carlo (QMC) simulations, based on the stochastic series expansion formulation and on the directed-loop algorithm [28]. The simulations are systematically done at temperatures low enough (typically $T \sim J/L$) so as to remove significant thermal effects. The truncation of the local Hilbert space up to a maximum bosonic occupancy $n_{\max}$ is accurately done to avoid significant truncation errors (we went up to $n_{\max}=6$ for the largest fillings considered, $n \approx 3$). When averaging over different realizations of the QP potential, we have considered typical samples of 100–300 realizations. The QMC method we use is formulated in the Fock-state basis, so that all quantities which are diagonal in that basis (density, compressibility, etc.) are straightforwardly evaluated. The superfluid density is estimated through the fluctuations of the winding number W in the world-line configurations produced during the simulation [29], $\rho_s = \langle W^2 \rangle L/(2\beta J)$. Finally we calculate the momentum distribution

$$n(k) = \frac{1}{L}\sum_{lm} e^{iq(l-m)}\langle b_l^\dagger b_m \rangle, \tag{6}$$

obtained through the statistics of the directed-loop update [30,32]. Most of the QMC results of the paper are based on a standard *grand-canonical* algorithm, already well documented in the literature [28,30]. In Secs. VI–VIII we also present results obtained with a novel *canonical* algorithm with multiple directed loops, designed for the calculation of higher-order off-diagonal correlators. The description of the algorithm is beyond the scope of the present paper, and we postpone it to a forthcoming publication.

III. HARD-CORE LIMIT

In this section we present exact results for the hard-core case. The study of hard-core bosons in QP potentials has been recently initiated by Refs. [17,18]. Remarkably the exact mapping onto spinless fermions, Eq. (4), allows one to exploit the large body of results produced several years ago in the context of tight-binding models in a QP potential [16]. In particular, focusing on localization phenomena, a fundamental result is the so-called Aubry-André conjecture [13,16] stating that for $V_2 < 4J$ all single-particle states are extended, while for $V_2 > 4J$ all states are localized. The single-particle spectrum is organized in *bands*, which have a fractal support [12] (Cantor set) at the critical value $V_2 = 4J$.

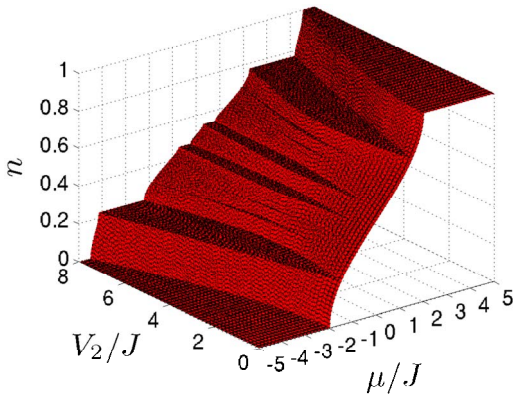

FIG. 1. (Color online) Density for hard-core bosons in a QP superlattice; here, the system size is $L=1076$ and the incommensuration parameter is $\alpha = 830/1076$.

According to Eq. (4), the properties of the many-body system, and in particular its elementary excitations, are easily read out from the single-particle spectrum for periodic and antiperiodic boundary conditions. Figure 1 shows the atom density, while Fig. 2 shows the superfluid density and compressibility of the hard-core boson system as a function

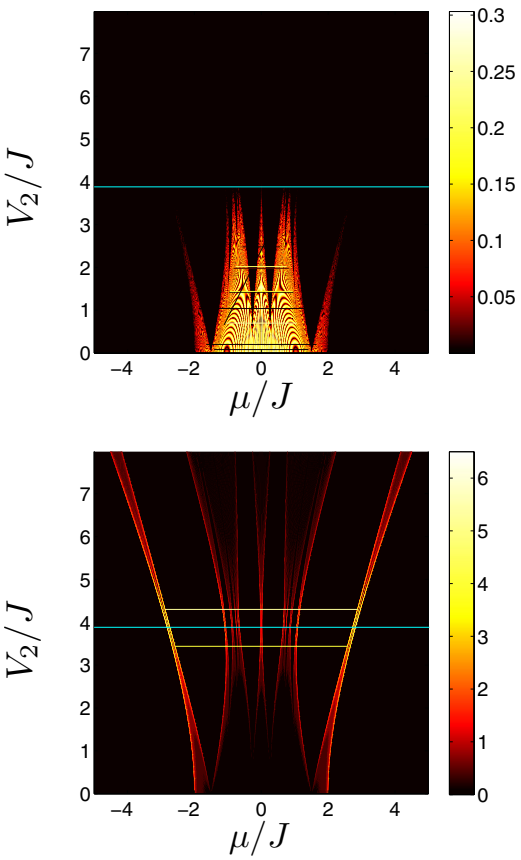

FIG. 2. (Color online) Superfluid density (upper panel) and compressibility (lower panel) for hard-core bosons in a QP superlattice (parameters as in Fig. 2). The cyan horizontal line marks the critical value $V_2/J=4$ for the localization transition. The "zebra"-like features in the superfluid density are finite-size effects.

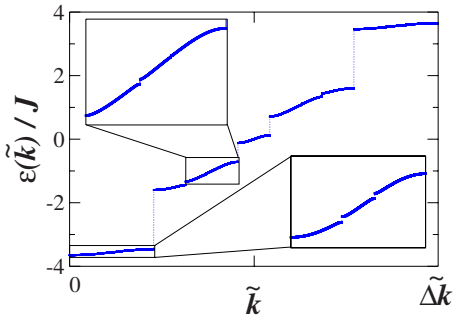

FIG. 3. (Color online) Dispersion relation for a single particle in a QP potential of intensity $V_2/J=6$.

of the chemical potential and strength of the QP potential. The first quantity clearly show the occurrence of plateaus at incommensurate values (the most prominent ones being at $n\approx 0.229$ and at $n\approx 0.457$), signaling the presence of IBI phases. The latter two quantities exhibit a highly nonmonotonic dependence on the chemical potential μ at all finite values of V_2. The compressibility is clearly finite for a finite single-particle density of states at the chemical potential, $\rho^{(+)}(\mu)$ $[\rho^{(-)}(\mu)]$ for periodic [antiperiodic] boundary conditions depending on the number of particles as in Eq. (4); in this case, an extra particle can be added to the system by an infinitesimal change of the chemical potential. As for the superfluid density ρ_s, in a truly periodic system (namely, in a *commensurate* superlattice) this quantity is directly proportional to the group velocity of the single-particle dispersion relation at the chemical potential [33], as it immediately emerges from the definition of ρ_s as a response function to an infinitesimal phase twist in the operators, $b_l \rightarrow b_l \exp(i\delta l)$: namely, $\rho_s = (L/2J)\partial^2 E/\partial\delta^2|_{\delta=0}$ (E is the total energy of the system). Hence ρ_s is finite when the chemical potential is inside a band and zero otherwise [33]. In the case of a QP potential the direct connection between superfluid density and group velocity breaks down formally, as quasimomentum is not a good quantum number anymore and the single-particle states do not have consequently a well-defined group velocity. Even though the new quantum number $\tilde{k}$ labeling the single-particle states is not, strictly speaking, the momentum, the single-particle spectrum $\epsilon(\tilde{k})$ shows a dependence on $\tilde{k}$ which is reminiscent of that of a system in a periodic potential (see Fig. 3 for an example); in particular, close to a gap, the dependence of $\epsilon(\tilde{k})$ on $\tilde{k}$ is extremely weak and it vanishes at the band edge. If $\tilde{k}_{\text{edge}}$ is the quantum number of the edge state and if the quantum numbers are defined on an interval $\Delta\tilde{k}$, the quantum number of the closest state at lower energy will be $\tilde{k}^{(-)}_{\text{edge}} = \tilde{k}_{\text{edge}} - \Delta\tilde{k}/L$. A vanishing derivative of the energy spectrum with respect to $\tilde{k}$ implies then that

$$\frac{[\epsilon(\tilde{k}_{\text{edge}}) - \epsilon(\tilde{k}^{(-)}_{\text{edge}})]}{\Delta\tilde{k}/L} \rightarrow 0 \tag{7}$$

for $L\rightarrow\infty$; this means in turn that the energy difference $\epsilon(\tilde{k}_{\text{edge}}) - \epsilon(\tilde{k}^{(-)}_{\text{edge}})$ vanishes faster than $1/L$ in the thermodynamic limit. Consequently, when the chemical potential sits close to the band edge, the infinitesimal perturbation induced by a change in the boundary conditions from periodic to antiperiodic is going to mix states with an energy difference decreasing faster than $1/L$, and hence is it going to produce an energy change $E^{(-)} - E^{(+)}$ which obeys the same scaling. This then leads to a vanishing ρ_s as defined in Eq. (5).

On the contrary, for states corresponding to the middle of the bands the perturbation induced by a change in the boundary conditions will cause an energy shift scaling like $1/L$, leading to a finite ρ_s, provided that such states are affected at all by a *local* perturbation [34]—namely, provided they are *extended* [35]. Hence in Fig. 2 it is not surprising to observe a finite ρ_s corresponding to a finite compressibility for $V_2/J<4$ and to observe an indentically vanishing ρ_s regardless of the chemical potential for $V_2/J>4$, as, according to the Aubry-André conjecture, the critical point marks a transition from all extended to all localized states. This means that the hard-core boson system exhibits an alternation of SF and IBI phases for $V_2/J<4$, while for $V_2/J>4$ the alternation is between IBI phases and BG phases, displaying a finite compressibility in the absence of superfluidity.

IV. SOFT-CORE CASE

When releasing the hard-core constraint for the bosons, we lose the possibility of describing the system via free fermionic quasiparticles and a fundamental question arises on the fate of the phase alternation described in the previous section. For $V_2=0$ the phase diagram of the one-dimensional Bose-Hubbard model in the grand-canonical ensemble is well known [36,37], and it features an extended SF region at large J/U ratio and a succession of Mott lobes with integer fillings for lower J/U. Similarly to what is done in the absence of a QP potential, we study the phase diagram in the $(J/U, \mu/U)$ plane, which is also directly relevant for the intepretation of the behavior in a trapped system (see Sec. VI). For definiteness, we choose to study the system with a *strong* QP potential compared to the interparticle repulsion; namely, we choose $V_2=U$ in Eq. (1). Under this condition the MI regions are completely destabilized, given that the Mott gap is upper-bounded by U and hence the Mott phase is not going to survive the application of an Hamiltonian term which is systematically larger than the gap. Hence the only insulating phases surviving in the $V_2=U$ case will generically be compressible or incompressible *incommensurate* ones—namely, insulating phases with incommensurate filling factors—as shown in Fig. 4.

We map out the phase diagram for $V_2=U$ via grand-canonical quantum Monte Carlo simulations for a single lattice size $L=126$ and for a commensurate approximant $\alpha=97/126$ to the incommensuration parameter used in the experiment [10]. The phase factor ϕ of Eq. (2) is set to 0 for simplicity. Similarly to the soft-core case, the characterization of the phases is carried out by investigating the compressibility κ and the superfluid density ρ_s. The phase diagram emerging from the simulations is of extreme complexity, and several observations are in order, as it will be discussed extensively in the next subsection, Sec. IV A. It is important to stress that what we present in Fig. 5 is the

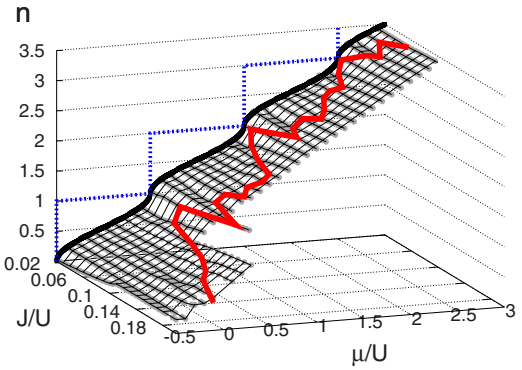

FIG. 4. (Color online) Density plot for the phase diagram of the Bose-Hubbard model in a QP potential with strength $V_2=U$ ($L=126$). The red line marks the boundary between the insulating (small-J/U) and the superfluid (large-J/U) regions. The bold black line is the density curve in the atomic limit $J\to 0$ (notice that it is reported on the graph minimum $J/U=0.02$ for comparison with the numerical data at finite J). The dashed blue line shows the same curve for $V_2=0$ and for a shifted chemical potential $\mu\to\mu-U/2$ (see text).

phase diagram for a *finite-size* system and for a *single realization* of the QP potential (namely, a single value of ϕ); we will see in Sec. IV A how to overcome these limitations. In the phase diagram, in the absence of superfluidity, we observe a patchwork of compressible and incompressible insulating regions. In Fig. 5 we indicate with a blue dot a point in parameter space which is found to be incompressible.

A. Finite-size effects

Before discussing the fundamental features of the phase diagram, it is important to stress the following technical point. At *strictly* zero temperature, the number of particles, N, is a constant, given that it is a good quantum number of the Bose-Hubbard Hamiltonian in an external potential; the variation of N upon changing the chemical potential μ proceeds in integer steps, and hence the compressibility, giving the slope of such curve, is simply a succession of δ peaks. Given a system size L and a μ value such that the ground-state particle number is N, the energy gaps between the

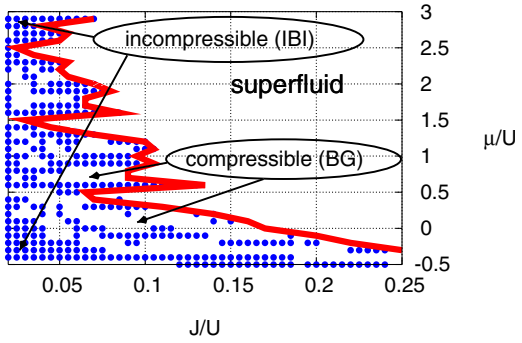

FIG. 5. (Color online) Phase diagram of the Bose-Hubbard model in a QP potential with strength $V_2=U$ ($L=126$). Blue dots mark points which are found incompressible. Other symbols as in Fig. 4.

ground state in the N-particle sector and the ground states in the sectors with $N+1$ and $N-1$ particles can either scale to a constant for $L\to\infty$, in which case the system is *incompressible* in the thermodynamic limit, or they can scale to 0, in which case the system is compressible in that limit and the apparent incompressibility at finite L is a finite-size artifact. The quantum Monte Carlo method we make use of is intrinsically a finite-T approach, and even for a finite-size system, it can deliver a finite compressibility value if T is larger than the finite-size gap between different particle number sectors. In the simulation of, e.g., the Bose-Hubbard model without QP potential, one can rely on the (finite-temperature) compressibility to approximately locate the zero-temperature phase boundary between the compressible SF phase and the incompressible MI phase. The error that one can make in that case is to ascribe to the SF phase that portion of the MI phase whose gap is comparable to the temperature, but this is definitely a tolerable error as long as the topology of the phase diagram is simple (e.g., one single boundary line dividing two extended phases).

In the case under consideration, we are far from simplicity. In fact, Figs. 4 and 5 are apparently conflicting, since Fig. 4 seems to suggest an insulating region with a smoothly varying $n(\mu)$ over most of the parameter space—namely, an insulating region which is mostly compressible—whereas Fig. 5 suggests rather the opposite—namely, that a dominant part of the insulating phase diagram is incompressible. The compressibility data upon which Fig. 5 is based are obtained at a temperature ($T=J/96$) which is possibly lower than most finite-size gaps in the insulating region, so that the incompressible portion of the finite-size phase diagram is overestimated with respect to that in the thermodynamic limit. Raising T is not recommendable, given that in this way narrow incompressible domains in the phase diagram, expected in principle on the basis of the hard-core limit (see Sec. III), might be washed out if their gap becomes lower than the temperature. Hence, given the tight alternation of compressible and incompressible regions, the finite-size or finite-temperature error that one can make in overestimating the ones over the others is considerable.

One possible strategy to circumvent this intrinsic *conundrum* of finite-size simulations is based on the following observation. If a truly irrational α is taken in Eq. (2), increasing the system size leads to a self-averaging QP potential; namely, the properties of the system in the thermodynamic limit become independent of the phase ϕ. This means that increasing the system size toward the thermodynamic limit at fixed ϕ is equivalent to averaging over the phase ϕ on a sample of fixed size L, as long as L is chosen to be much larger than any correlation length ξ in the system. Hence, away from the critical line between the SF phase and the insulating one(s) (where $\xi\to\infty$), the behavior of the system in the thermodynamic limit can be obtained by averaging the finite-size results over all possible values of ϕ. In practice, for a compressible region of the phase diagram one expects that, for some values of ϕ, the finite-size gap between different N sectors becomes smaller than the selected temperature, so that a finite compressibility is recovered on average. This numerical procedure is computationally demanding, and we limit it to two selected cuts through the phase diagram,

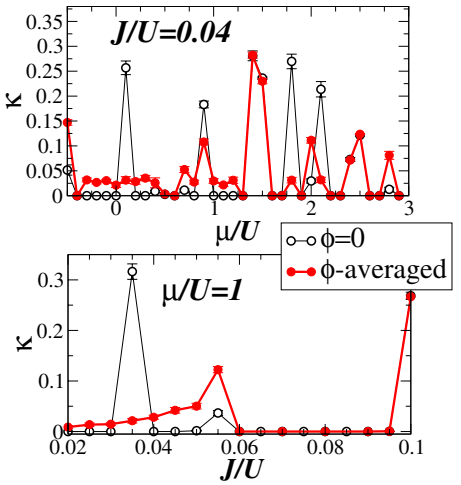

FIG. 6. (Color online) Compressibility for the Bose-Hubbard model in a QP potential with fixed spatial phase $\phi=0$, compared with the same quantity averaged over ϕ fluctuations.

one for fixed $J/U=0.04$ and one for fixed $\mu/U=1$. The results are shown in Fig. 6: they confirm the expectation that the fixed-ϕ phase diagram overestimates the incompressible regions, but at the same time they confirm the presence of sizable incompressible (IBI) regions, in tight alternation with the compressible ones (BG). Given the finiteness of the grid used in the $(J/U,\mu/U)$ plane to sample the phase diagram, we cannot exclude that an even tighter alternation between IBI and BG regions exists among the dots, possibly revealed by a finer mesh.

B. Emergence of the incompressible regions

The tight alternation of compressible and incompressible insulating regions upon varying the chemical potential reveals that there are several "magic" incommensurate fillings at which a *quasiparticle* band is filled, similarly to what happens to the exact fermionic quasiparticles in the hard-core limit. In the compressible BG regions, on the other hand, varying the chemical potential leads to variations in the fillings, and all the newly added particles are effectively localized by the QP potential and by the interaction with the density background of the other particles. Figure 4 shows the filling of the lattice in the region of phase diagram we sampled numerically, along with the atomic limit both for the case $V_2=U$ and for the case $V_2=0$. It is to be noticed that the QP potential of Eq. (2) is symmetric around zero energy, and in particular the local chemical potential in its minima takes the value $\mu-U/2$; hence, a correct comparison with the case $V_2=0$ requires one to consider a Bose-Hubbard Hamiltonian with a shifted chemical potential $\mu\to\mu-U/2$. The presence of the strong QP potential alters significantly the density curve in the atomic limit, washing out the steps associated with Mott lobes in the case $V_2=0$, given that the system has lost translational invariance and the average density can take all possible values. Therefore a seemingly continuous curve emerges, with integer densities appearing only at semi-integer values of μ/U; this behavior reflects the broad distribution of local chemical potentials in the sites of the QP

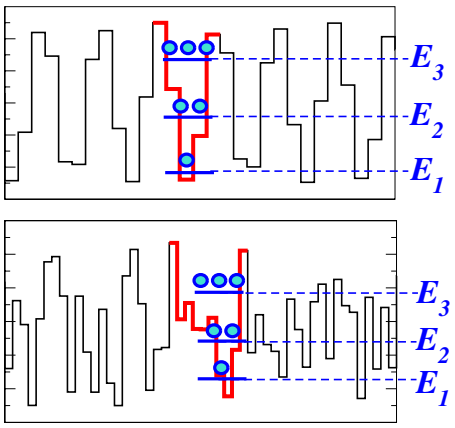

FIG. 7. (Color online) Schematic depiction of the *random-atomic-limit* approach for a QP potential (upper panel) and for a truly random one (lower panel). This approach subdivides the system into potential wells, here marked in red, and it diagonalizes the problem of one, two, and three particles confined in each well, extracting the corresponding ground-state energies E_1, E_2, and E_3. Such energies are then used to reconstruct the density of states of the system for low filling.

potential, gradually occupied upon increasing μ until the nth "shell" is completed when an integer density n is reached. The density of atomic states in a QP potential is peaked around the energies $\pm V_2/2$ (see Figs. 7 and 8 below), as expected given that these are the values where the potential has minimum derivative, and consequently the density curve has maximum slope around $\mu=(m+1/2)U$ (with m integer). Hence the atomic limit picture suggests a *finite* compressibility for all chemical potentials, and intuitively one would expect the compressibility to stay finite *a fortiori* in the presence of quantum fluctuations, turned on through the hopping term. This would be generally true in the case of a *truly random* potential, on average over the possible realizations of the potential or in the thermodynamic limit. Yet, in the case of a pseudorandom potential, one of the main quantum effects is to break the continuous classical many-body spectrum into *bands*. This mechanism is discussed in the next section.

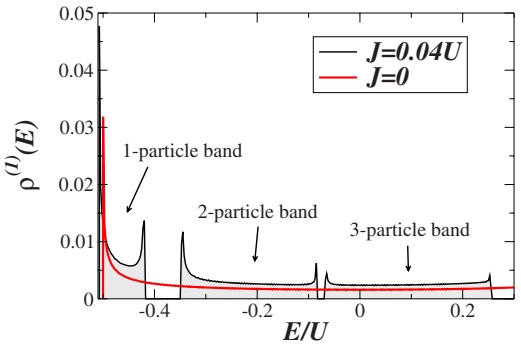

FIG. 8. (Color online) Random-atomic-limit result for the effective single-particle density of states of a Bose-Hubbard model in a QP potential with $V_2=U$ and over a large system size ($L=10^6$). The quantum case of $J/U=0.04$ is compared with the classical limit $J=0$.

V. TRUE DISORDER vs PSEUDODISORDER

In this section we describe the formation of bands in the quantum *many-body* spectrum of the Bose-Hubbard model in an incommensurate potential making use of a generalization of the atomic limit which includes the first quantum correction in a *nonperturbative* way. The central idea is to subdivide the QP potential in uncorrelated wells, which are assumed to be independent from each other in the case $V_2/J \gg 1$, and to diagonalize the N-boson problem in each of the wells. We call this approach the *random atomic limit*. This approach not only reproduces the main features of the $n(\mu)$ curve and of the associated many-body density of states at low fillings, but it also nicely elucidates the fundamental difference between a pseudorandom potential and a truly random one and the fundamental mechanism leading to BG physics. Finally it suggests a strategy to emulate the behavior of a truly random potential making use of a combination of *two* superimposed QP potentials.

A. Random atomic limit

We propose here an approximate treatment of the strongly interacting Bose-Hubbard model in an intense QP potential, $U=V_2 \gg J$, in the case of low fillings. The idea is that the QP potential subdivides the lattice into potential wells between which tunneling is negligible when not assisted by the interaction (namely, for low fillings) and hence interwell coherence can be neglected within a good approximation. Hence the Bose-Hubbard model in the grand canonical ensemble can be treated as follows: (a) isolate each potential well, cutting the chain at the location of the maxima delimiting the well itself, and diagonalize the Bose-Hubbard Hamiltonian in this potential for $N=1,2,\ldots$ particles, finding the ground state energies E_1, $E_2,\ldots$; (b) due to the QP potential and to the interaction U, adding a second particle to the well costs more energy than adding the first, and so for the third: namely, $E_1<E_2-E_1<E_3-E_2-E_1<\cdots$. Hence one can build an effective single-particle density of states (DOS) $\rho^{(1)}(E)$ by accumulating the energy costs for the addition of a single particle to each well, $\epsilon_1=E_1$, $\epsilon_2=E_2-E_1$, $\epsilon_3=E_3-E_2-E_1$, etc. We moreover normalize the DOS to unity: namely,

$$\rho^{(1)}(E)=\frac{1}{N_{\text{states}}}\sum_{i=1,2,3,\ldots}\sum_{\epsilon_i}\delta(E-\epsilon_i). \tag{8}$$

The filling for a given μ is simply found by integrating $\rho^{(1)}(E)$ up to μ, similar to the case of noninteracting fermions.

For $J=0$, and in the case $U=V_2$ and $n<1$, any new particle added to the ground state of the system occupies the least energetic site that remains empty. Hence the DOS $\rho^{(1)}(E)$ in that case simply reflects the distribution of the on-site energies in the potential, which is a continuous one in the interval $[-U/2,U/2]$. The quantum corrections to it, obtained for up to $N=3$ particles per well, are shown in Fig. 8; the calculation was made for a large sample of the QP potential considered so far ($J/U=0.04$), such that self-averaging of the system properties is guaranteed. We observe the striking feature of the opening of *gaps* in the DOS, defining effective bands which are populated by the gradually added particles. It is important to stress that the states associated with these bands are localized and that the nature of these bands is determined by the many-body physics inside each well. In particular the first band is associated with states in singly occupied wells and the finite energy cost to add an extra particle to any of the well in the system causes the appearance of a gap to the next band. The potential-energy cost of adding an extra particle is completely compensated for by the gain in chemical potential; hence, the only remaining energy cost which prevents particle addition is purely quantum in nature and it comes from the loss of kinetic energy in the first particle when adding a second one to the well. The same reasoning applies when adding a third particle, which gives rise to a further band, etc. In periodic systems, the emergence of Bloch bands is due to the strong scattering of traveling matter waves with wave vector at the edges of the Brillouin zone; here, we have on the contrary the appearance of bands associated with tightly localized particles and band gaps emerging due to a strong correlation among the particles.

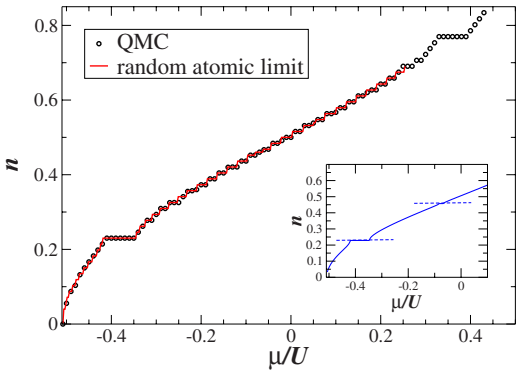

FIG. 9. (Color online) Density curve for the Bose-Hubbard model in a QP potential with $\alpha=97/126$, $J/U=0.04$, and $V_2=U$ on a system size $L=126$. Inset: random-atomic-limit calculation on a large system size ($L=10^6$).

The opening of gaps in the effective single-particle DOS leads to plateaus in the $n(\mu)$ curves and hence to incompressible phases at special, incommensurate fillings. The $n(\mu)$ curve obtained in the random atomic limit is compared with the QMC results at $J/U=0.04$ and for low fillings in Fig. 9. We observe that the random-atomic-limit calculation reproduces very well all the fine details of the $n(\mu)$ curve from QMC: (a) it perfectly captures the large plateau which corresponds in Fig. 8 to the gap between the one-particle band and the two-particle band, occurring at a filling $n=0.229\ldots$ (also observed in the hard-core limit; see Fig. 1 [38]); (b) moreover, it also correctly captures the finite-size plateaus due to the discrete jumps in the particle number in the $n(\mu)$ curve. Here the significance of finite-size issues in the determination of the phase diagram of the system is particularly evident: in fact, for the $L=126$ chain the finite-size gaps are completely masking the second plateau in the $n(\mu)$ curve at density $n=0.457\ldots$, which on the contrary is clearly exhibited in the random-atomic-limit calculation on a large system size (inset of Fig. 9).

B. From pseudodisorder to true disorder: The two-color quasiperiodic potential

The discussion of the previous section allows us to clearly identify the origin of the incompressible behavior in the insulating regime of the QP potential. At some specific fillings the addition of an extra particle requires one to locally squeeze the particles already present in the QP potential wells, and this squeezing costs a finite amount of kinetic energy which translates into a gap over the ground state. Actually the energy cost for the addition of a single particle can be arbitrarily lowered if the potential wells are made arbitrarily large, given that in this way the kinetic energy cost for the particles already present can be minimal. In a well of characteristic size l a particle has a confinement energy $\sim\hbar^2/2ml^2$; the addition of a second particle, which is ideally impenetrable to the first one, roughly lowers the effective space available to the latter to $l/2$ and hence it increases its confinement energy to $\sim 4\hbar^2/2ml^2$. Hence the energy increase scales to 0 as l^{-2} when increasing the well size.

The QP potential has a characteristic length scale given by the quasiperiod of the QP potential—namely, $l=2\pi/(k_{\mathrm{L}}-k_{\mathrm{QP}})=(1-\alpha)^{-1}$—coming from the beating between the incommensurate cosine potential at wave vector $k_{\mathrm{QP}}=2\pi\alpha$ and the underlying lattice (formally at a wave vector $k_{\mathrm{L}}=2\pi$). Potential wells cannot exceed this length scale, and therefore the confinement energy scale is bounded from below. This means that gaps to particle addition at particular incommensurate fillings are unavoidable in the system. Moreover, working with a fixed number of particles at the same special filling, a gap opens to particle-hole excitations: intrawell excitations are clearly gapped due to the finite size of the well, and particle-hole excitations which cause the transfer of a particle from a well to another are also gapped, due to the chemical potential mismatch between particle and hole.

One fundamental feature of a truly random potential, on the other hand, is the absence of an upper bound for the extent of potential wells and hence the possibility of always adding a particle to the system at an infinitesimal energy cost or, at fixed filling, to introduce a particle-hole excitation at arbitrarily low energy. This feature, based on the statistics of rare regions (large wells), is at the heart of the gaplessness of the BG phase [5,39,40]. To corroborate this statement quantitatively, we apply the random-atomic-limit approach described in the previous subsection to a truly random potential with a random on-site energy evenly distributed over the interval $[-U/2,U/2]$. We use two different criteria to identify the potential wells: C*riterion 1*. A potential well is delimited by two successive local maxima with positive height. *Criterion 2*. A potential barrier is identified with a local maximum whose height over the previous local minimum is larger than $U/2$, and we hence identify a well with a region between two such barriers (see Fig. 7). Criterion 1 is less restrictive than criterion 2, and it surely underestimates the size of the potential wells. Yet in the case of the QP potential of Eq. (2) both criteria would lead to the same identification of the potential wells as the one used in the previous subsection. As shown in Fig. 10, regardless of the criterion the resulting effective single-particle DOS $\rho^{(1)}$ associated with many-body intrawell states is continuous for a truly random potential and all gaps are removed by the absence of an upper bound in the well length l.

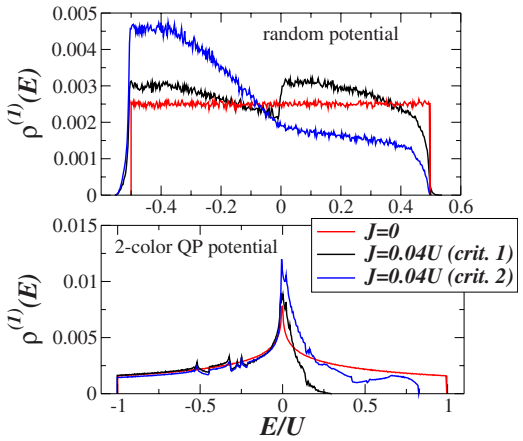

FIG. 10. (Color online) Density of states from the random atomic limit for a truly random potential (upper panel) and for a two-color QP potential (lower panel). The random potential takes values over the interval $[-U/2,U/2]$, while the two-color QP potential has $V_2=U$. For both systems $L=10^6$. Results from two different criteria for the identification of the potential wells (see text) are compared with the classical limit ($J=0$).

From the point of view of the cold-atom experiments, realizing optically an ideal white-noise potential requires one to superimpose a large number of standing-wave components with different wave vectors and with the same weight; this translates into the need of a large amount of lasers at different frequencies and with the same intensity, which is extremely demanding. Hence an interesting question, both at the fundamental level and at the practical one, is the following: can we mimic *de facto* the physics of a system of bosons in a truly random potential by just using a finite number of superimposed standing waves or, in more suggestive terms, *how many colors do we need for a pseudorandom potential to call it disorder*?

As discussed above, our goal is to realize a pseudorandom potential with the minimal amount of Fourier components giving rise to a continuous many-body spectrum—namely, not exhibiting incompressible IBI phases. The guiding principle is that of realizing a potential whose spatial features are richer than those of a simple QP potential, such that larger wells are realized giving rise to intrawell excitations at lower energy and such that states with a different number of particles in different wells become quasidegenerate, giving rise to low-energy interwell particle-hole excitations.

From this perspective we explore the most straightforward generalization to the QP potential so far considered; namely, we add a second incommensurate component to the QP potential of Eq. (2), having the same intensity as the first one, thus realizing a *two-color QP potential*

$$g^{(2)}(i;\alpha,\phi,\alpha',\phi')=\cos^2(\pi\alpha i+\phi)+\cos^2(\pi\alpha' i+\phi')-1. \tag{9}$$

In what follows we take $\alpha'=71/126=0.563\,49\ldots$. Figure 10 shows the random-atomic-limit calculation for such a poten-

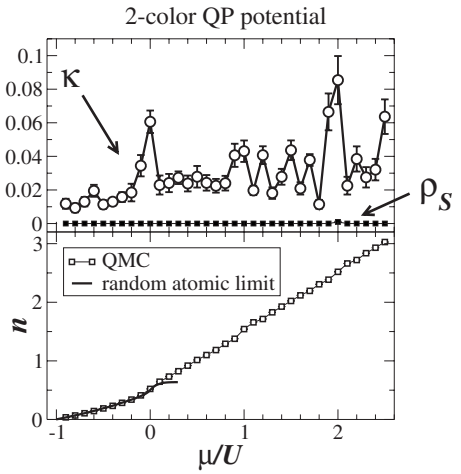

FIG. 11. Compressibility and superfluid density (upper panel) and total density (lower panel) for the Bose-Hubbard model in a two-color QP potential, Eq. (9), on a $L=126$ lattice with $\alpha=97/126$, $\alpha'=71/126$, $V_2=U$, and $J/U=0.04$. The QMC results are averaged over independent fluctuations of the spatial phases ϕ and ϕ'.

tial on a large sample size (which makes the particular values of the phases ϕ and ϕ' irrelevant). For both criteria of well identification we obtain a gapless single-particle DOS—namely, no incompressible phase at low filling—opposite to the case of a simple QP potential. This encourages us to explore the behavior of the system over a larger filling interval, making use of QMC simulations. Figure 11 shows the compressibility, superfluid density, and total density for the Bose-Hubbard model in a two-color QP potential for a large μ/U range; the results shown are averaged over independent fluctuations of the ϕ,ϕ' phase, hence exploiting the whole statistics associated with the potential of Eq. (9) and removing finite-size effects, as discussed in Sec. IV. Noticeably, the density curve at low fillings ($n\lesssim 0.5$) agrees very well with that predicted by the random-atomic-limit calculation. Furthermore, over the larger grid of chemical potentials and fillings which is accessible to QMC simulations (we went up to $n\approx 3$) we find a finite compressibility everywhere, generally coexisting with insulating behavior (only around $\mu/U\approx 2$ a tiny superfluid density shows up). Hence this particular *pseudodisordered* potential features a continuous BG phase *without* intermediate IBI regions. This means that the Bose-Hubbard model in a two-color QP potential seems to capture some of the fundamental physical features of the classic dirty-boson problem [5]. It remains to be seen whether the transition from SF to BG in such a potential belongs to the same universality class as that of the system in a truly random potential and whether the absence of incompressible regions in the phase diagram applies to the whole parameter space and to any combination of the incommensurability parameters α and α': we leave these questions open for future investigations.

VI. TRAPPED SYSTEM AND LOCAL-DENSITY APPROXIMATION

In the following sections we discuss the behavior of a system of bosons in an incommensurate optical superlattice

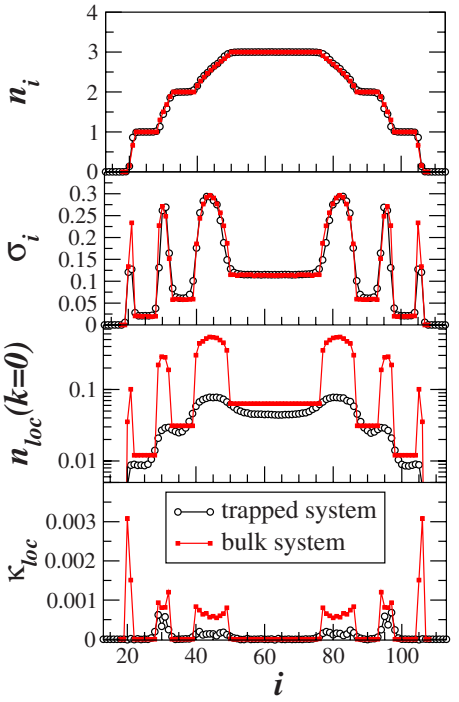

FIG. 12. (Color online) Local quantities for a Bose-Hubbard system in a trap with parameters $U=20J$, $V_t=0.0014\ U$, $\mu_{\rm trap}=2.5\ U$, and $L=126$ (from top to bottom panel: density, on-site particle-number fluctuations, local coherent fraction, and local compressibility), compared with the same quantities for a bulk system with a chemical potential matching the local one in the trap.

in the presence of a parabolic trapping potential, to make contact with the experimental setup of current optical-lattice experiments [10,23]. Hence we consider the Hamiltonian

$$\mathcal{H}_{\rm trap}=\mathcal{H}_0+V_t(i-i_0)^2, \tag{10}$$

where V_t is the strength of the trapping potential and i_0 is the center of the trap.

In the absence of an incommensurate potential, the behavior of the Bose-Hubbard model in a trap is generally connected to that of the bulk system via a *local-density approximation* [30,41,42]. Here we discuss how that approximation holds only partially in the presence of an incommensurate potential and how the behavior of the trapped system has to be regarded in its own respect.

A. Bose-Hubbard model without QP potential

In the presence of a smoothly varying potential—namely, under the assumption that $V_t\ll J,U$—recent works [30,41,42] have shown that a local-density approximation fully applies to the standard Bose-Hubbard model [Eq. (1) with $V_2=0$]; namely, the local properties in the trap, such as, e.g., the density, can be directly related to those of the homogeneous system in the grand-canonical ensemble by matching the local chemical potential in the trap, $\mu_i=\mu_{\rm trap}-V_t(i-i_0)^2$, to that of the homogeneous system. A similar calculation is shown in Fig. 12, where the local density $\langle n_i\rangle$ and the on-site particle number fluctuations

$$\sigma_i = \langle n_i^2 \rangle - \langle n_i \rangle^2 \tag{11}$$

are compared for a trapped system and a bulk system. Good agreement between the data for the trapped system and those for the bulk system is observed away from the crossover regions between a locally SF and a locally MI region, while in the crossover regions the data for the trapped system have generally less sharp features with respect to those for the homogeneous one. This can be intuitively understood by noticing that finite-size effects are typically most pronounced close to the critical boundaries between different phases, where discontinuities and singularities are rounded off by the finiteness of the system. In the trapped system the finite-size effects are not only given by the overall trapping potential, but most significantly by the finiteness of those regions whose local chemical potential corresponds to critical boundaries between MI and SF in the homogeneous case.

Despite the finite-size corrections, the above results lead typically to interpret the various regions in the trapped system as *locally superfluid* or *locally Mott insulating* depending on the corresponding phase at the same chemical potential in the phase diagram of the bulk system. This conclusion is particularly confirmed when looking at the *local condensate fraction*

$$n_{\mathrm{loc},i}(k=0) = \frac{1}{L}\sum_j \langle b_i^\dagger b_j \rangle \tag{12}$$

and at the *local compressibility*, introduced in Ref. [31],

$$\kappa_{\mathrm{loc,i}} = \frac{\beta J}{L}\sum_j \left(\langle n_i n_j \rangle - \langle n_i \rangle \langle n_j \rangle\right). \tag{13}$$

Notice that in the homogeneous bulk system with global condensate fraction $n(k=0)$ and global compressibility κ, we have that $n_{\mathrm{loc},i}(k=0)=n(k=0)/L$ and $\kappa_{\mathrm{loc},i}=\kappa/L$. From Fig. 12 we see that the behavior of both $n_{\mathrm{loc},i}(k=0)$ and $\kappa_{\mathrm{loc},i}$ in the trapped system follows qualitatively that of the global quantities in the bulk system. In particular it is important to notice that both $n_{\mathrm{loc},i}(k=0)$ and $\kappa_{\mathrm{loc},i}$ are actually nonlocal quantities and their final values depend not only on the local chemical potential at point i, but also on the properties at other points in the trap and in particular on the total number of particles in the trap. Thus a close agreement with the bulk data is generally not expected, in particular whenever the correlation functions $\langle b_i^\dagger b_j \rangle$ and $(\langle n_i n_j \rangle - \langle n_i \rangle \langle n_j \rangle)$ become long ranged in the bulk system: namely, in the SF phase and at the SF-to-MI boundary, respectively. Nonetheless, $n_{\mathrm{loc},i}(k=0)$ and $\kappa_{\mathrm{loc},i}$ capture the short-range behavior of those correlators in the trapped system around the point i; therefore, their local enhancement expresses the fact that phase coherence between the points in those regions is strong, which is typical of a locally superfluid islands, and that particle number fluctuations in those regions are strongly correlated, which is a signature of the existence of low-energy and long-wavelength density modes. Conversely a vanishing local compressibility manifests a local gap to particle-hole excitations and it is typically accompanied by a lower local phase coherence. These two combined observations form the basis to the LDA interpretation of local MI and SF phases in a trap. This interpretation is fundamental to conclude that the MI phase is realized at all in the trapped system, with a halo of SF surrounding it; indeed, only an infinite repulsion U and an infinitely steep trap would allow to realize a *pure* MI in the trap.

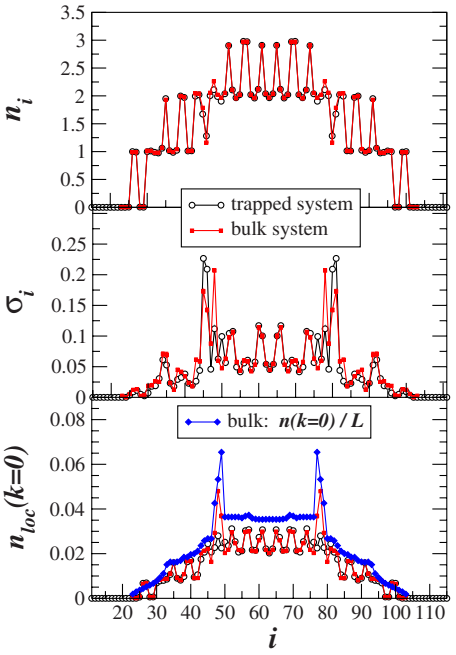

FIG. 13. (Color online) Local density, particle-number fluctuations, and coherent fraction (from top to bottom) for a Bose-Hubbard system in a trap plus QP potential, with parameters $U=30J$, $V_t=0.0014\ U$, $\mu_{\mathrm{trap}}=1.8\ U$, $V_2=U$, and $L=126$. The above quantities are compared to those of the bulk system with matching *local* potential [Eq. (14)].

B. Bose-Hubbard model with QP potential

When introducing the incommensurate cosine potential as in Eq. (1), the picture becomes significantly more complex. We will henceforth limit our discussion to the case $V_2=U$ already discussed in Secs. IV and V—namely, the case in which the MI phase is completely removed from the phase diagram and substituted by a variety of incommensurate gapped and gapless insulating phases.

In the presence of an incommensurate cosine potential, even the bulk system becomes inhomogeneous, and hence the LDA has to be rephrased as the approximation relating the properties of a point in the trapped system to those of a point in a bulk system experiencing the same local chemical potential, resulting from the global chemical potential *plus* the cosine potential; in mathematical terms, we have to identify a site i_{trap} of the trapped system with a site i_{bulk} of the bulk system such that

$$\mu_{\mathrm{loc}} = \mu_{\mathrm{trap}} - V_t(i_{\mathrm{trap}} - i_0)^2 - V_2 g(i_{\mathrm{trap}};\alpha,\phi) = \mu_{\mathrm{bulk}} - V_2 g(i_{\mathrm{bulk}};\alpha,\phi), \tag{14}$$

where μ_{trap} and μ_{bulk} are the global chemical potentials for the trapped and bulk systems, respectively. Figure 13 compares the results for the bulk and trapped systems following

the prescription of Eq. (14) in the case of a strongly interacting system in a deep incommensurate potential, $U/J=V_2/J=30$. With these parameter values the bulk system lies in the insulating region of the phase diagram for a broad range of chemical potentials. In what follows we consider $\mu_{\rm trap}/U=1.8$ so that the local chemical potential in the trapped system, which is upper-bounded by the above value, experiences a superfluid region of the bulk phase diagram (Fig. 5) only around the value $\mu_{\rm loc}/U=1.5$.

Despite the high inhomogeneity of both the bulk and trapped systems, we generally observe a good quantitative agreement between their respective data for the local average density, local density fluctuations, and local coherent fraction. For the interval of chemical potentials spanned by $\mu_{\rm loc}$ only two nearby critical points are present in the bulk phase diagram around $\mu_{\rm loc}/U=1.5$, so that, away from those two points, the system is deep in an insulating region with a short correlation length, and finite-size effects are therefore not severe. The problematic aspect of the LDA in the presence of the QP potential is nonetheless the subsequent interpretation of the trapped system as locally exhibiting a phase of the bulk system. In particular, what is the meaning of a *local Bose glass*?

In this respect, the examination of the local compressibility compared with the global one is illuminating. As shown in Fig. 14, the *local* compressibility of the trapped system is in strong disagreement with the *global* one, and it is generally vanishing when the global one is not. This is not at all surprising in a strongly inhomogeneous system, in which the global compressibility is due to the local response of disconnected regions to the variation of the chemical potential, and it is related to the existence of localized low-energy particle-hole excitations. Although a region in the trap might be at a chemical potential which would correspond to a BG phase in the bulk phase diagram, it is very likely that such a region does *not* correspond to the region of the bulk system that is hosting the locally quasigapless excitation and which is hence exhibiting a finite local compressibility. This is indeed the case for what depicted in Fig. 14, where we show the local compressibility of the bulk system for a chemical potential corresponding in the trap to a locally *incompressible* region: as observed there, the bulk system has a finite compressibility at that chemical potential, coming from the local compressibility of regions which do *not* correspond to the ones reproduced in the trap (shaded areas). Hence it is evident how the finite-size effects induced by the trap are drastically altering the local behavior of the system with respect to that of the bulk one.

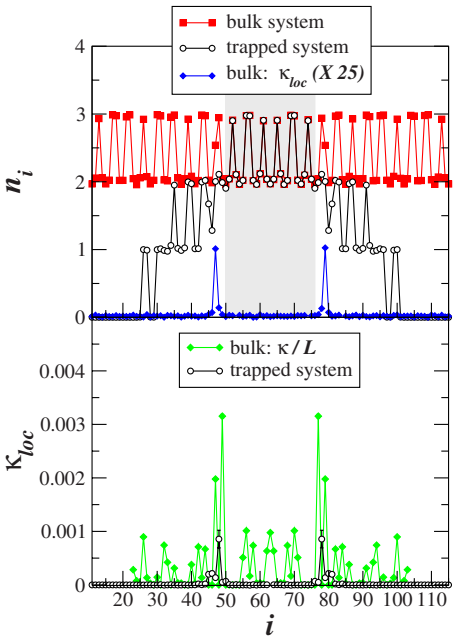

FIG. 14. (Color online) Upper panel: local density of the trapped system compared with local density and local compressibility of a bulk system with chemical potential $\mu_{\rm bulk}=1.8U$. The region where trapped and bulk density profiles match is emphasized by the shaded area (notice that the chemical potentials $\mu_{\rm trap}$ and $\mu_{\rm bulk}$ match perfectly only at the trap center, but the variation of $\mu_{\rm trap}$ due to the trapping potential is slow around the center). The regions exhibiting a finite local compressibility in the bulk system are seen to fall out of the region of matching densities, and consequently the trapped system is locally incompressible (see following panel). Lower panel: local compressibility of the trapped system compared with the global compressibility of the bulk system. All other parameters as in Fig. 13.

C. Structure of the particle-hole excitations

The above results require to discard the LDA picture of the trapped system locally mimicking the behavior of the bulk system when it comes to the BG phase. At the same time, the very picture of a local realization of collective quantum phases in a trapped system might be a limiting point of view. As pointed out in Sec. V, the existence of gapless particle-hole excitations, originating from rare regions in the system, is at the core of the BG phase: e.g., accidentally degenerate regions separated by a potential barrier, for which tunneling creates a pair of quasidegenerate symmetric and antisymmetric superposition states similarly to the double-well problem, or rare regions with a locally uniform or periodic potential, which host local low-energy excitations.

As we have seen, the inhomogeneity of the QP potential is what causes a trapped system to fail in reproducing locally the global properties of a bulk system at the same chemical potential. At the same time it is conceivable that, in the presence of the trap, accidental degeneracies might occur between local quasiparticle states residing at *different* trapping potentials—namely, accidental degeneracies which are not observed in the bulk system. To directly investigate this possibility, we have run a canonical Monte Carlo simulation in which we add particles progressively to the system. We then define *effective* quasiparticle and quasihole states $\psi^{(N)}_{\rm quasi\text{-}p}$ and $\psi^{(N)}_{\rm quasi\text{-}h}$ such that their associated density distribution corresponds to the density variation of the system by adding or removing a particle, respectively:

$$|\psi^{(N)}_{\rm quasi\text{-}p}(i)|^2 = n_i^{(N+1)} - n_i^{(N)}, \tag{15}$$

$$|\psi^{(N)}_{\text{quasi-h}}(i)|^2 = n_i^{(N)} - n_i^{(N-1)}. \quad (16)$$

Looking at the spatial structure of the quasiparticle and quasihole states corresponding to the same particle number N, we generally obtain information about the structure of the particle-hole excitations of the system at particle number N.

In fact, starting from $N-1$ particles, the energy cost of adding an extra particle is given by the kinetic energy plus the interaction of the extra particle with the background of the $N-1$ particles already present in the system and analogously for adding an extra particle to go from N to $N+1$. If the density variation associated with growing the particle number from $N-1$ to N happens in a different spatial region with respect to the variation caused by growing the number from N to $N+1$, then the quasihole state $\psi^{(N)}_{\text{quasi-h}}$ and the quasiparticle state $\psi^{(N)}_{\text{quasi-h}}$ are nonoverlapping. In the presence of short-range interactions as in the Bose-Hubbard model, this implies that the addition of the Nth particle does not influence the background with which the $(N+1)$th particle interacts, which implies, in more concise terms, that the quasiparticle and quasihole are not interacting. Thus, working at particle number N, the creation of a quasihole in state $\psi^{(N)}_{\text{quasi-h}}$ and of a quasiparticle in state $\psi^{(N)}_{\text{quasi-p}}$ represents the true lowest-energy particle-hole excitation of the system, with energy $\Delta E_N = \Delta E_{\text{p-h}} = E^{(0)}_{N+1} + E^{(0)}_{N-1} - 2E^{(0)}_N$ ($E^{(0)}_N$ is the ground-state energy for the system with N particles).

If, on the contrary, the quasiparticle and quasihole states for particle number N do overlap, then in principle the energy $\Delta E_{\text{p-h}}$ needs a correction coming form the interaction in order to be identified with the energy of the elementary particle-hole excitation. Yet, if $\Delta E_{\text{p-h}}$ is found to be small ($\ll U$ for definiteness), then the interaction between the Nth added particle with the background of $N-1$ particles, entering in the $E^{(0)}_N - E^{(0)}_{N-1}$ difference, has essentially the same energy as that of the interaction between the $(N+1)$th particle and the background of N particles, entering in the $E^{(0)}_{N+1} - E^{(0)}_N$ difference; this in turn implies that the Nth particle minimally alters the interaction between the $(N+1)$th particle and the remaining $N-1$; namely the quasiparticle and the quasihole states are again effectively independent, and they are moreover essentially degenerate. If not even the above condition on $\Delta E_{\text{p-h}}$ is satisfied, we can still generally assume that, in the presence of repulsive interactions, $\Delta E_{\text{p-h}}$ represents an upper bound to ΔE_N [43] and that the spatial structure of the true particle-hole excitations is approximately reproduced by that of $\psi^{(N)}_{\text{quasi-h}}$ and $\psi^{(N)}_{\text{quasi-p}}$.

In the case of a trapped system without QP potential, the quasiparticle and quasihole states are shown in Fig. 15 for a selected range of particle numbers N and the associated particle-hole gap $\Delta E_{\text{p-h}}$ is shown in Fig. 16. We generally observe that the quasiparticle and quasihole states reside in the locally superfluid regions, as expected from the information on the local compressibility. For the particular density we have chosen in Fig. 15 the system exhibits two such regions, at local filling $n<1$ on the wings and at filling $n>1$ in the center. We generally observe three different types of particle-hole pairs, with $\Delta E_{\text{p-h}} \ll U$ in all cases: (a) pairs where quasiparticle and quasihole both reside in the center of the trap—these are the excitations which more closely mimic those of a finite-size SF system; (b) pairs where quasiparticle and quasihole both reside in the wings of the trap—these states correspond to the symmetric and antisymmetric superpositions of the left- and right-localized states in the wings, and the particle-hole gap $\Delta E_{\text{p-h}}$ is minimal in this case, because the large barrier provided by the intermediate MI region leads to quasidegeneracy (see for instance the case of $N=55,56,61,62$); (c) particle-hole pairs with a particle residing in the wings and the hole in the center or vice versa. The excitations (b) and (c) are *specific* to the trapped system; in particular, it is noteworthy that quasidegeneracy exists between states related to different trap regions, and hence the picture of local phases described in the previous paragraph does not extend to excitations.

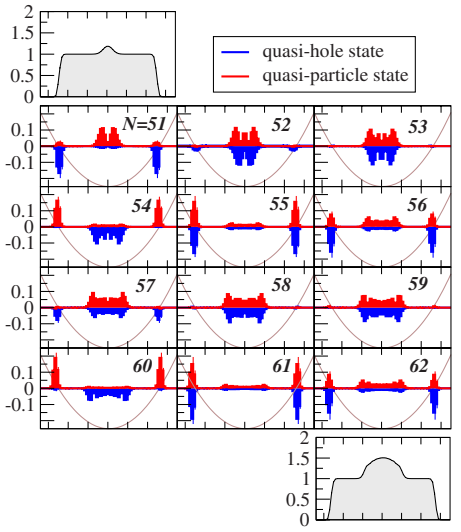

FIG. 15. (Color online) Central panels: quasiparticle $[|\psi^{(N)}_{\text{quasi-p}}(i)|^2]$ and quasihole $[-|\psi^{(N)}_{\text{quasi-h}}(i)|^2]$ densities for the Bose-Hubbard model in a trap at various particle numbers N and with parameters $U=20J$ and $V_t=0.0014U$. A rescaled picture of the parabolic trap is reported in each panel for reference. Upper and lower panels: total density profile associated with the minimum ($N=51$) and maximum ($N=62$) number of particles shown here.

In the presence of a strong QP potential with $V_2=U$, the structure of the excitations changes drastically, although some of the features observed before persist: namely, the cross talk between different trap regions. Figure 17 shows the spatial structure of quasiparticle and quasihole states and Fig. 18 the particle-hole gap. It is evident that the strong QP

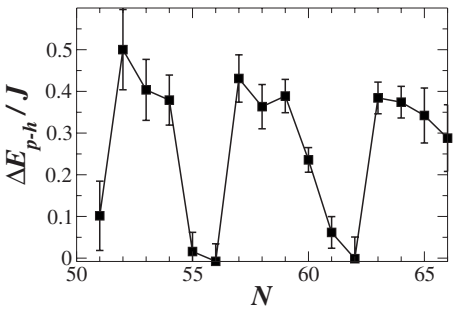

FIG. 16. Particle-hole gap $\Delta E_{\text{p-h}}$ for the Bose-Hubbard model in a trap. Parameters as in Fig. 15.

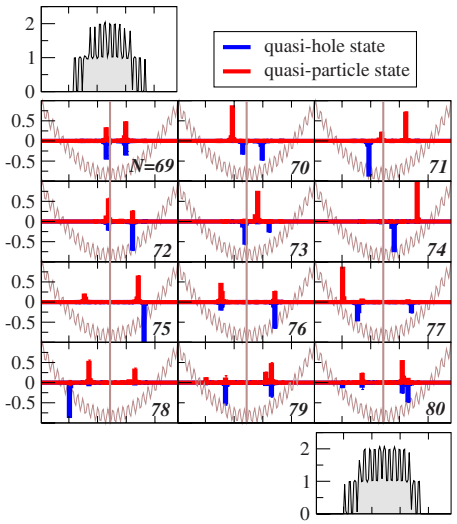

FIG. 17. (Color online) Central panels: quasiparticle $[|\psi^{(N)}_{\text{quasi-p}}(i)|^2]$ and quasihole $[-|\psi^{(N)}_{\text{quasi-h}}(i)|^2]$ densities for the Bose-Hubbard model in a trap plus QP potential at various particle numbers N, with $V_2=U=20J$. Other parameters as in Fig. 15. A rescaled picture of the parabolic trap plus the QP potential is reported in each panel for reference, together with the trap axis. Upper and lower panels: total density profile associated with the minimum ($N=69$) and maximum ($N=80$) number of particles shown here.

potential leads to tight localization of the added particles and holes in the system, typically around a few lattice sites; delocalization of the quasiparticle and quasihole states onto two disconnected regions is due to the symmetric-antisymmetric combination of quasidegenerate localized states (as before, these combinations give rise to the lowest particle-hole gaps, such as, e.g., for $N=69$, 72, 76, etc.). Furthermore, quasiparticle and quasihole states are very often *decoupled* spatially (see, for instance, the cases $N=70,71,73,74,75,77,78$). This means that the lowest-energy particle-hole excitations are not at all confined to equipotential regions, but they can be associated with accidental quasidegeneracies of quasiparticle and quasihole states between regions at quite different trapping potentials. Hence the notion of "local (quasi)gaplessness" is too restrictive, and the picture of a local BG, which we have seen to break down in the previous discussion, can be superseded by the possibility of having a *global* trapped BG, in which low-energy particle-hole excitations, albeit corresponding to the

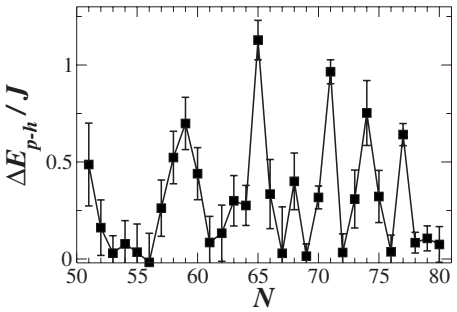

FIG. 18. Particle-hole gap $\Delta E_{\text{p-h}}$ for the Bose-Hubbard model in a trap plus QP potential. Parameters as in Fig. 17.

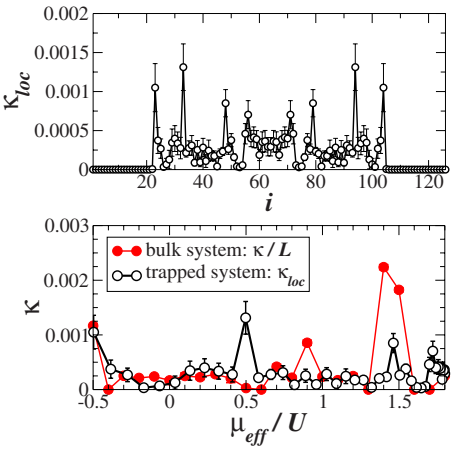

FIG. 19. (Color online) Upper panel: phase-averaged local compressibility for the Bose-Hubbard model in a QP potential, with parameters $U=25J$, $\mu_{\text{trap}}=1.8U$, and $V_t=0.0014U$. Lower panel: the phase-averaged local compressibility of the trapped system is compared to the phase-averaged global compressibility of the bulk system (see also Fig. 6) by matching the average chemical potentials: here $\mu_{\text{eff}}=\mu_{\text{trap}}-V_t(i-i_0)^2$ for the trapped system and $\mu_{\text{eff}}=\mu_{\text{bulk}}$ for the bulk system.

transfer of a quasiparticle between two localized states, can also occur between distant points in the trap [44].

D. Bose glass in the trap: One-color vs two-color QP potential

In Sec. VI we have seen that for a single realization of the QP potential the concept local BG (in the sense of the LDA) breaks down due to significant finite-size effects. This feature is actually generic of inhomogeneous systems, and we expect it to hold also for a single realization of a truly random potential. The concept of local BG can be nonetheless recovered *on average* over the statistics of the (pseudo)disordered potential. In the specific case of a QP potential, one can randomize its spatial phase as in Sec. V. Interestingly, from the point of view of optical-lattice experiments, averaging over fluctuations of the spatial phase of the QP potential is inevitable when averaging the results over different experimental runs. In fact, the spatial phase can be fixed over the duration of a single run, but it is typically changing from run to run [45].

Randomizing the spatial phase of the QP potential implies that the potential profile can randomly "slide" along the trap. If a region of the trap experiences a local chemical potential which corresponds to that of a BG phase in the bulk phase diagram, there is in principle a finite probability that, by random sliding of the QP potential, a region hosting a gapless particle-hole excitation in the bulk system will appear in the trap, so that *on average* that portion of the trap acquires a finite local compressibility. Figure 19 compares the data, averaged over ϕ fluctuations, of the rescaled global compressibility κ/L for the bulk system (already shown in Fig. 6) with those of the local compressibility in the trap, plotted as a function of the effective chemical potential induced by the trap, $\mu_{\text{eff}}=\mu_{\text{trap}}-V_t(i-i_0)^2$. This time we observe that, upon ϕ averaging, most compressible phases in the bulk are gen-

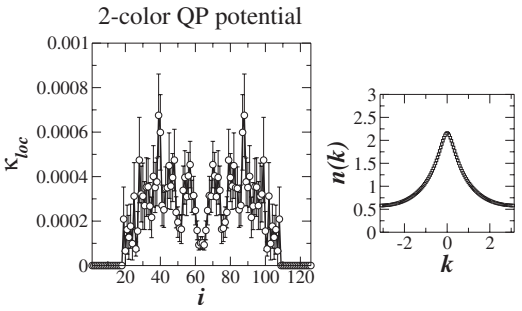

FIG. 20. Left panel: local compressibility of the Bose-Hubbard model in a trap plus a two-color QP potential, averaged over fluctuations of the spatial phases of the two colors. Here $V_t=0.0014U$, other parameters as in Fig. 11. Right panel: momentum distribution for the same system (on a lattice of $L=126$).

erally mirrored by locally compressible phases in the trap and even that there exist locally compressible phases in the trap which correspond to *incompressible* phases in the bulk. This suggests that the finite compressibility in this case is associated with low-energy excitations which are specific of the trapped system, as discussed in the previous section.

The above results finally suggest the following conclusion: a truly random potential or a pseudorandom potential, giving rise *on average* to a BG phase for a continuous range of chemical potentials in the phase diagram of the bulk system, should also be able to give rise *on average* to a locally compressible phase on *all* the points of the trapped system. To verify this statement in a particular case, we look at the two-color QP potential of Sec. V in a trap. This potential is seen to satisfy the above condition on the bulk compressibility over an extended range of chemical potentials (see Fig. 11). Figure 20 shows the local compressibility of this system, averaged over spatial-phase fluctuations. In contrast with what observed in Figs. 14 and 19, we have here a finite local compressibility everywhere in the trap, on average over ϕ fluctuations. At the same time the system exhibits a very low coherence which allows to rule out quasicondensation [46]. Hence we conclude that this system perfectly realizes a BG *all over the trap.*

VII. RELEVANT EXPERIMENTAL OBSERVABLES FOR THE TRAPPED SYSTEM

In this section we show results for two relevant observables that are currently accessible to time-of-flight measurements in optical-lattice experiments: namely, the first-order [10,23] and second-order [25,47–49] coherence of the bosons. The first-order coherence contains the information on the momentum distribution, Eq. (6). The second-order coherence contains instead information on the correlations between the momentum distribution fluctuations (also called *noise correlations*):

$$G(k,k') = \langle n(k)n(k')\rangle - \langle n(k)\rangle\langle n(k')\rangle. \tag{17}$$

What is customarily measured in experiments [25,49] is actually the average correlations between the populations at two momenta differing by a value q, normalized to the factorized correlator:

$$I(q) = \frac{\sum_{k\in \mathrm{FBZ}} \langle n(k)n(k+q)\rangle}{\sum_{k\in \mathrm{FBZ}} \langle n(k)\rangle\langle n(k+q)\rangle}. \tag{18}$$

In order to evaluate $G(k,k')$ and $I(q)$ we need in general to be able to evaluate four-point off-diagonal correlators of the type $\langle b_i^\dagger b_j b_l^\dagger b_m\rangle$ within QMC simulations and to successively Fourier transform them. This is possible within a *double-directed-loop* canonical algorithm that we explicitly developed for this purpose, in which the evaluation of the above-cited four-point correlator is performed during the update whenever the four ends of the two loops find themselves at the same time slice on the sites i, j, l, and m. Details of the algorithm will be reported elsewhere. We investigate the evolution of the first- and second-order coherence upon increasing the strength of the incommensurate cosine potential. We fix the ratio U/J to two different values $U/J=5$ and 10, which give rise to two different states at zero QP potential in a trap of strength $V_t/J=0.0014U$.

For $U/J=5$ the trapped system with $V_2=0$ exhibits a high coherent fraction and the application of the QP potential has the effect of suppressing coherence, driving the system through a superfluid-to-incommensurate-insulator crossover, as clearly shown in Fig. 21. We then compare the evolution of the momentum distribution with that of the density profile upon increasing V_2 (also shown in Fig. 21), which is not directly measurable in the current experiments. We notice that the strongest suppression of the coherent peak at $k=0$ corresponds roughly to the value of V_2 at which the incommensurate potential introduces unoccupied sites in the central region of the trap, fragmenting the many-body state into droplets.

Along the superfluid-to-insulator crossover the system traverses a *modulated superfluid* phase, in which the coherent fraction remains significant while the density profile acquires a strong modulation due to the external potential. This modulation is only marginally revealed in the momentum distribution by two satellite peaks at the incommensurate beating momenta $k_{\mathrm{inc}}=\pm 2\pi(1-\alpha)$ (see also Ref. [33] for a similar signature in commensurate superlattices). This effect can be understood as an effective reduction of the first Brillouin zone, due to the longer (quasi)period imposed by the incommensurate potential; yet its signature is possibly too weak to be observed in current optical-lattice experiments. It is also to be observed that such signature becomes unobservable in the strongly insulating regime, where the momentum distribution becomes essentially featureless.

Nonetheless, as shown experimentally in Refs. [25,49], the fluctuations of the momentum distribution, captured by Eqs. (17) and (18), have a momentum structure which reflects directly the Fourier transform of the density-density correlations. Indeed, for a pure Fock state $|\{n_i\}\rangle$ one can easily show that

$$I(q) = 1 + \frac{N}{L}\delta_{q,0} + \frac{N}{L^2}S(q), \tag{19}$$

where $S(q)=(1/L)\Sigma_{ij}\langle n_i n_j\rangle$ is the static structure factor and N is the total number of particles. In a more general superpo-

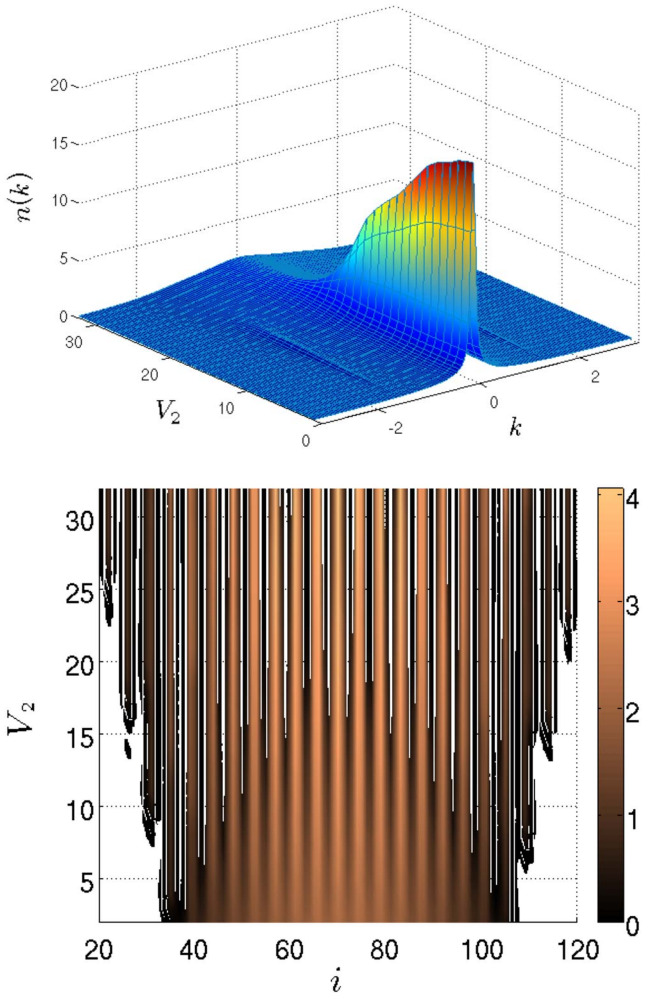

FIG. 21. (Color online) Upper panel: momentum distribution for the Bose-Hubbard model in a trap ($N=100$, $U=5J$, $V_t=0.0014U$, $L=140$) in a QP potential of increasing strength V_2 (here represented in units of J). Lower panel: false-color density plot for the same model; the false colors only apply to finite densities, while the white regions emphasize the points with zero density.

sition state $|\Psi\rangle=\Sigma_{\{n_i\}}c(\{n_i\})|\{n_i\}\rangle$ the above relation does not hold; nonetheless, if the state contains only one or a few dominant Fock components, the essential features of their related structure factor will be captured by the integrated noise correlations as in Eq. (18). Figure 22 shows the second-order coherence as a function of the intensity of the incommensurate potential. The central peak at $q=0$ shows a nontrivial evolution, with a large increase corresponding to the suppression of coherence and the consequent increase in the fluctuations $\langle n(k)^2\rangle$ at all momenta, which contribute to $I(q=0)$. But the most significant feature is the appearance of satellite peaks at $q=k_{\mathrm{inc}}$ and also at $q=2k_{\mathrm{inc}}$. The height of these peaks appears to saturate around the value of V_2 ($V_2/J\sim 20$) at which the coherence peak in the momentum distribution gets drastically suppressed, marking the fragmentation of the system into droplets.

Increasing the value of U/J to 10, the system at $V_2=0$ has a significantly lower coherence than in the case $U/J=5$. Interestingly the application of the QP potential appears to *increase* the coherence in the system, as shown in Fig. 23, an effect due to the simple fact that MI regions are destabilized by the application of the QP potential because they obviously do not display the right filling to minimize the potential energy. A similar effect of destabilization of the MI by an externally applied potential has been previously observed both in the case of a periodic potential [33,50] and in the case of a random one [51]. A further increase in the QP lattice leads to a similar crossover toward a deep incommensurate insulating state, as seen above for the case $U/J=5$. The second-order coherence shown in Fig. 24 also reveals a nonmonotonic behavior of the $q=0$ peak, where a suppression of momentum fluctuations is observed together with the enhancement of the $k=0$ peak. Satellite peaks at k_{inc} and $2k_{\mathrm{inc}}$ appear for large V_2 as in the case of a lower U/J ratio, but it is interesting to notice that the momentum structure of $I(q)$ is significantly less pronounced than in the case of $U/J=5$; in particular, the height of the satellite peaks has decreased with respect to that of the central one. To further illustrate this trend we have performed an exact calculation of $I(q)$ in the Fock-state limit $J\to 0$, whose results are shown in Fig. 24 and where it appears that in this limit the q-dependent struc-

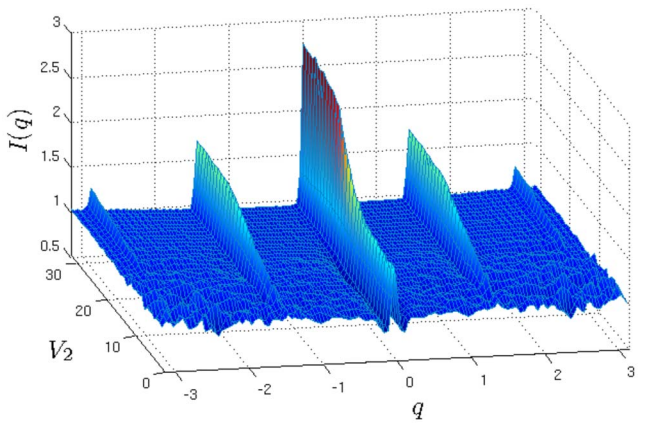

FIG. 22. (Color online) Noise correlations for the Bose-Hubbard model in a QP potential; model parameters as in Fig. 21.

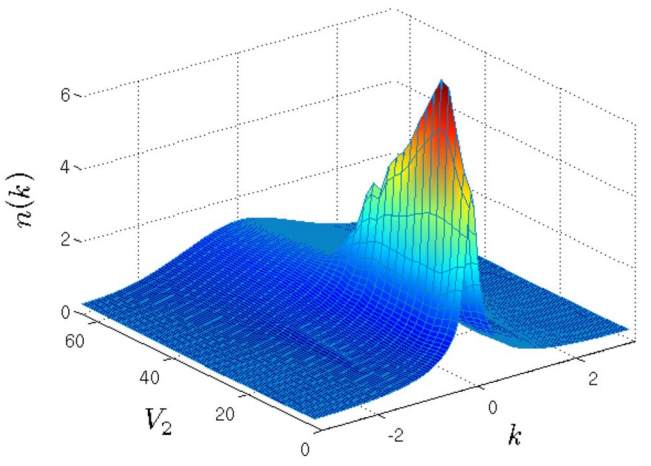

FIG. 23. (Color online) Momentum distribution for the Bose-Hubbard model in a QP potential with $U=10J$; other parameters as in Fig. 21.

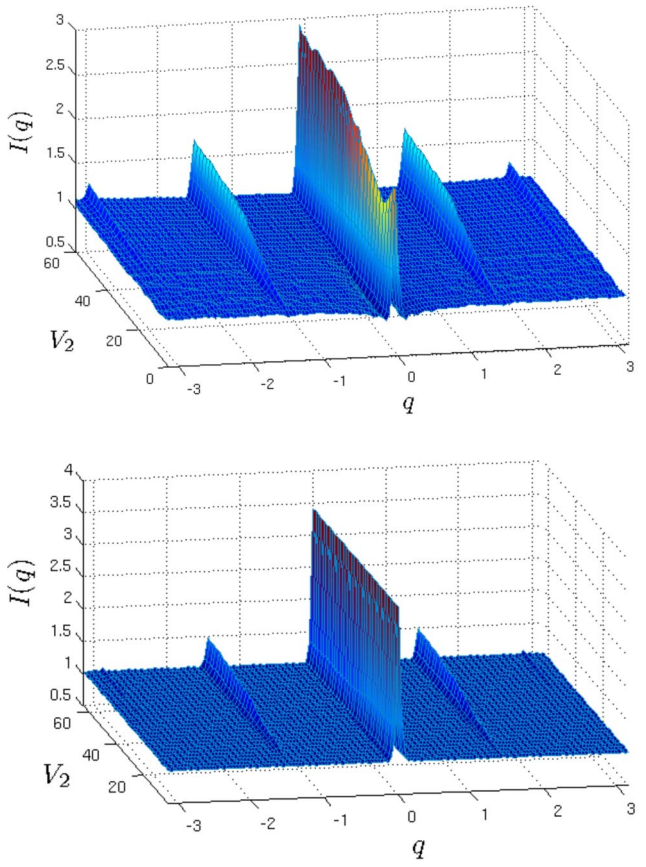

FIG. 24. (Color online) Upper panel: noise correlations for the Bose-Hubbard model in a QP potential with $U=10J$; other parameter as in Fig. 23. Lower panel: noise correlations for the classical limit of the above model, $J=0$. Here V_2 is in units of $U/10$.

ture of $I(q)$ is even weaker than in the finite-J case. Hence we can conclude that quantum fluctuations generally *enhance* the nontrivial q-dependent part of the $I(q)$ signal with respect to the $q=0$ peak.

In conclusion, we observe that the first- and second-order coherence provide full information about the diagonal and off-diagonal correlations in the system, and they clearly reveal the crossover (or finite-size transition) from a superfluid state to an incommensurate insulating state upon increasing the QP potential. The detection of the possibly unconventional nature of the insulating state—namely, the presence (albeit local) of BG regions—is nonetheless beyond the scope of these observables, and quantities that directly probe the low-energy particle-hole excitations are required, ideally the local compressibility as discussed in Sec. VI. Future work will present an experimental strategy to directly address this issue [52].

VIII. VALIDITY OF THE BOSE-HUBBARD MODEL IN AN INCOMMENSURATE POTENTIAL

Throughout the previous sections we have worked under the assumption that an incommensurate optical superlattice, realized in the experiments [10] by superimposing a primary and a secondary standing wave with incommensurate wavelength relation, can be fully described by a simple incommensurate cosine potential added to the Bose-Hubbard Hamiltonian, as in Eq. (1). This means that the only effect of the secondary optical lattice is assumed to be a shift of the local energy of the Wannier functions associated with the lowest Hubbard band of the primary lattice. Yet the frequency inside each potential well of the superlattice changes in general with respect to that of the single-color lattice and, most importantly, the relative distances between consecutive wells are also shifted [53]. These effects modify in principle the shape of the Wannier functions, leading to a modulation of the U parameter, and the overlap between the Wannier functions associated with two adjacent sites, leading to a modulation of the J parameter.

Here we recall the well-known derivation [22] of the Bose-Hubbard model from the most general second-quantized Hamiltonian of a set of interacting bosons in an external potential, which reads

$$\mathcal{H} = \int d^3r\, \psi^\dagger(\boldsymbol{r})\left(-\frac{\hbar^2}{2m}\nabla^2 + V_{\mathrm{opt}}(\boldsymbol{r})\right)\psi(\boldsymbol{r}) + g\int d^3r\, \psi^\dagger(\boldsymbol{r})\psi^\dagger(\boldsymbol{r})\psi(\boldsymbol{r})\psi(\boldsymbol{r}), \tag{20}$$

where ψ and $\psi^\dagger$ are bosonic field operators, $g=4\pi a_s\hbar^2/m$ with m the mass of the bosons and a_s the s-wave scattering length, and $V_{\mathrm{opt}}(x)$ is the optical potential applied to the atoms. Following the experimental setup of Fallani *et al.* [10], hereafter we assume that V_{opt} can be written as

$$V_{\mathrm{opt}}(\boldsymbol{r}) = V_{\parallel}(x) + V_{\perp}(y,z), \tag{21}$$

$$V_{\perp}(y,z) = s_{\perp}[\cos^2(k_1 y) + \cos^2(k_1 z)]E_r + \frac{1}{2}m\omega_{\perp}^2[(y-y_0)^2 + (z-z_0)^2], \tag{22a}$$

$$V_{\parallel}(x) = s_1\cos^2(k_1 x)E_r + s_2\cos^2(k_2 x+\phi)E_r + \frac{1}{2}m\omega_{\parallel}^2(x-x_0)^2. \tag{22b}$$

$V_{\perp}$ creates a strong optical-lattice potential with wave vector $k_1=2\pi/\lambda_1$ in the y and z directions, defining tubes along the x direction, plus an overall parabolic confinement with frequency $\omega_{\perp}$. Hereafter we consider a strong transverse optical lattice, $s_{\perp}=40$, as obtained in recent experiments [10,24], which allows us to neglect the intertube hopping and to consider single tubes independently. The optical potential along the x direction features two optical lattices with incommensurate wave vectors $k_1=2\pi/\lambda_1$ and $k_2=2\pi/\lambda_2$, plus a parabolic confinement with frequency $\omega_{\parallel}$. For definiteness we take $\lambda_1=830$ nm, $\lambda_2=1076$ nm, and $m\omega_{\parallel}^2/2=0.0012E_r$ as in Ref. [10]. s_1, s_2, and $s_{\perp}$ are dimensionless amplitudes, and $E_r=(\hbar k_1)^2/2m$ is the recoil energy (associated with the primary lattice).

We then decompose the bosonic field operators onto an orthonormal basis of single particle wave functions localized around the minima of the optical potential in each tube:

$$\psi(\boldsymbol{r}) = \sum_i w_i(x) W_i(y) W_i(z) b_i, \tag{23}$$

where i runs over the minima. Neglecting the overlap between localized wave functions on nonadjacent minima, the Hamiltonian parameters of a general one-dimensional Bose-Hubbard Hamiltonian

$$\mathcal{H} = \sum_i \left[(J_{i,i+1} b_i b_{i+1}^\dagger + \text{h.c.}) + \frac{U_i}{2} n_i(n_i - 1) + V_i n_i \right] \tag{24}$$

can be obtained as usual, with parameters

$$J_{i,i+1} = \int dx\, w_{i+1}^*(x) \left[-\frac{\hbar^2}{2m} \frac{\partial}{\partial x} + V_\parallel(x) \right] w_i(x), \tag{25}$$

$$U_i = g \int dx |w_i(x)|^4 \int dy |W_i(y)|^4 \int dz |W_i(z)|^4, \tag{26}$$

$$V_i = \int dx |w_i(x)|^2 V_\parallel(x). \tag{27}$$

The W_i's are the Wannier functions associated with the lowest band of the periodic potential in the y and z directions, which can be conveniently approximated by Gaussians in the limit of a deep optical lattice. Along the x direction Bloch's theorem does not apply due to the incommensuration between the two optical-lattice components, so that Wannier functions cannot be properly defined. Hence we take the w_i to be the ground state of the potential obtained by a polynomial expansion (up to sixth order) of $V_\parallel(x)$ around the ith minimum and the so-obtained set of localized functions is further Gram-Schmidt orthogonalized. In absence of the λ_2 optical lattice, this approach provides hopping amplitudes $J_{i,i+1}$ in good agreement with the estimate coming from the solution of the Mathieu equation [54] and it improves significantly over a simple Gaussian approximation for the w_i's (see Fig. 25). In the case of the full incommensurate superlattice, this approach shows a significant site dependence of the hopping amplitudes $J_{i,i+1}$, with differences between different pairs of sites that can reach one order of magnitude for intense secondary lattices. This is due to a significant shift in the positions of the minima of the incommensurate optical superlattice with respect to the monochromatic lattice and to the exponential sensitivity of the hopping amplitude to such shifts. An example of the site dependence of the hopping amplitudes for an intense secondary lattice is shown in Fig. 26, together with the local energies V_i. In particular, it is evident that the modulation of the local chemical potential and of the local hopping are strongly correlated; namely, the amplitude of the hopping is maximum where the local energy V_i is also maximum. Hence the modulated hopping competes in principle with the localization effects induced by the QP V_i's, given that the local kinetic energy is minimized in proximity of the potential maxima. Yet, looking at the magnitude of the hopping modulation with respect to the dominant local potential modulation, it is clear that one can still confidently rely on the simple Hamiltonian (1) to capture the dominant low-energy features of the Hamiltonian (20). Figure 27 shows the relative fluctuations $\delta J / J_{\text{av}}$ associated

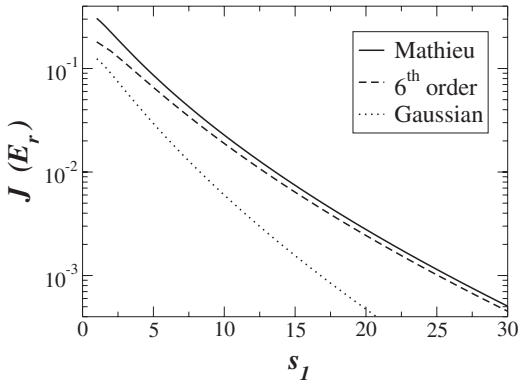

FIG. 25. Hopping amplitude J as a function of the lattice potential depth s_1 for a monochromatic optical lattice (both quantities are expressed in units of the recoil energy E_r). We show the estimate of J obtained through the solution of the Mathieu equation [54], $J/E_r = (4/\sqrt{\pi}) s_1^{3/4} \exp(-2\sqrt{s_1})$, through the calculation of the overlap integral Eq. (25) via sixth-order expansion of the optical potential (see text), and through the simple Gaussian approximation for the Wannier functions, $J/E_r = (\pi^2/4 - 1) s_1 \exp[-(\pi^2/4)\sqrt{s_1}]$.

with the modulation of $J_{i,i+1}$ around the average value J_{av} and their amplitude δJ compared with the energy scale of the potential created by the secondary lattice, $s_2 E_r$. Although the relative fluctuations can be extremely large and far exceed 100%, the energy range spanned by those fluctuations becomes negligible with respect to the energy scale of the potential, and hence the modulation of the hopping is not expected to alter significantly the behavior of the system for strong secondary lattices. As for the site dependence of the interaction U_i, we find that it reaches $\sim 10\%$ for the strongest secondary lattice considered in Fig. 27, so we discard it for simplicity in the following.

To quantitatively verify that the hopping modulation does not significantly affect the physics of the system, we have studied the first- and second-order coherence of the system with the full *ab initio* Hamiltonian (24) and compared the results to the case in which we neglect the hopping modulation: namely, Eq. (24) with $J_{i,i+1} = J = \text{const}$. The results are shown in Fig. 28 for the momentum distribution and in Fig. 29 for the noise correlations. We observe that taking into

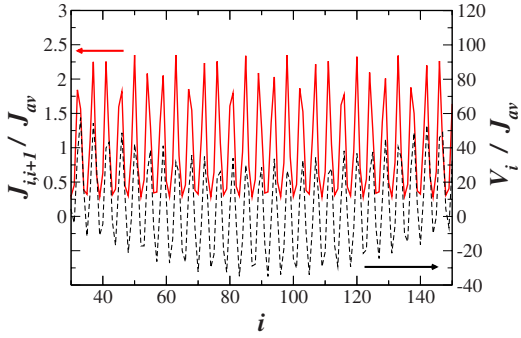

FIG. 26. (Color online) Site-dependent hopping amplitude $J_{i,i+1}$ and local potential V_i for the generalized Bose-Hubbard model, Eq. (24), derived from the microscopic Hamiltonian for bosons in an incommensurate optical superlattices. Here $s_1 = 8$, $s_2 = 3$, and $m\omega_\parallel^2/2 = 0.0012 E_r$.

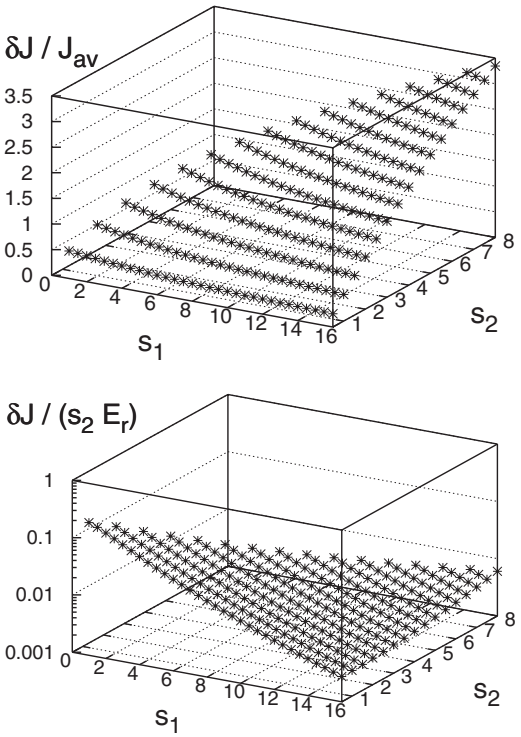

FIG. 27. Upper panel: relative fluctuations of the effective hopping amplitude $J_{i,i+1}$ for bosons in an incommensurate superlattices, as a function of the intensities s_1 and s_2 of the two superimposed standing waves. Lower panel: ratio of the hopping amplitude fluctuations over the potential energy of the secondary standing wave.

account the hopping modulation does not alter the most significant qualitative features of these observables. As for the momentum distribution, we observe that the hopping modulation leads to a stronger suppression of coherence for strong QP potentials; in the case of noise correlations, we see that the modulation of the hopping amplitude leads to a reduction of the signal at the incommensurate momentum $q=k_{\mathrm{inc}}$ and even more significantly of the one at $q=2k_{\mathrm{inc}}$, with respect to the central peak at $q=0$. For the first observation, a possible explanation is that the hopping modulation strongly suppresses hopping in the minima of the potential and hence the residual coherence of the particles trapped in those minima. As for the second observation, a reduction of the signal in the noise correlations is also compatible with a reduction of quantum fluctuations inside the potential wells, as observed in Sec. VII when taking the classical limit $J\rightarrow 0$ (see Fig. 24).

IX. SUMMARY AND CONCLUSIONS

In summary, we have presented an extensive numerical study of the physics of interacting lattice bosons in a quasiperiodic (QP) potential, in direct connection with recent experiments on cold bosons in incommensurate optical superlattices [10].

We have investigated the exactly solvable limit of hard-core repulsive bosons, where the system can be mapped onto noninteracting fermions, so that the well-known physics

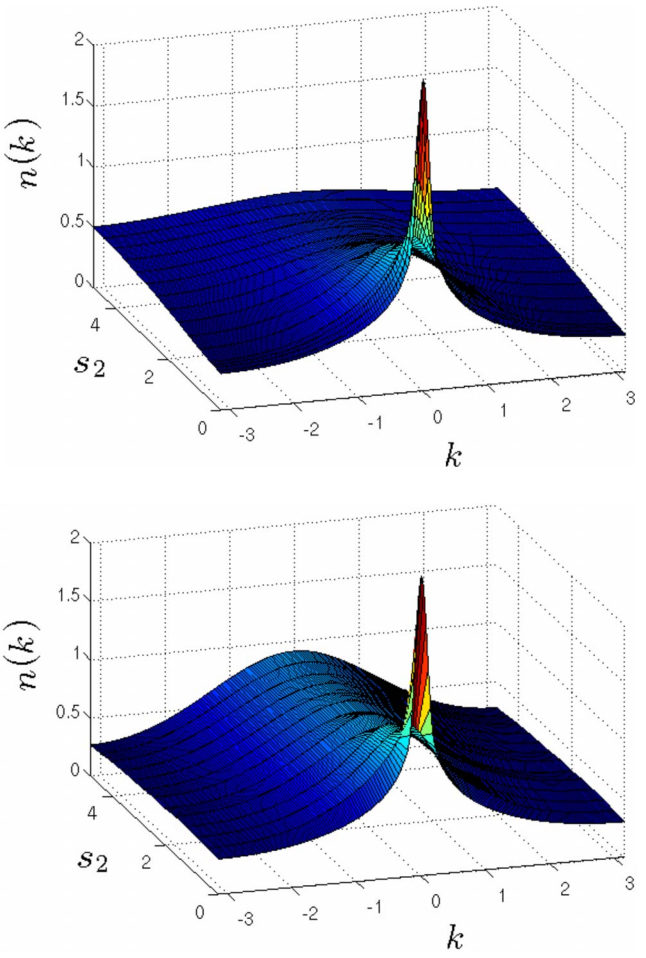

FIG. 28. (Color online) Upper panel: momentum distribution of $N=100$ bosons in an incommensurate superlattice with $s_1=8$ and variable s_2 ($s_\perp=40E_r$, $a_s=100a_0$ as in ^{87}Rb with $a_0=$Bohr radius and other parameters as in Fig. 26), calculated for the generalized Bose-Hubbard Hamiltonian (24). Lower panel: same quantity for the model, Eq. (24), *without* accounting for the hopping modulation, $J_{i,i+1}=J=$const. For both panels $L=180$.

[13,16] of one-dimensional particles in an incommensurate superlattice directly applies to the many-body system. There the emergence of gaps in the single-particle spectrum translates into the appearance of a gapped incommensurate band-insulator phase in the many-body phase diagram, together with the gapless Bose glass (BG) phase. This picture survives also in the more realistic case of soft-core interactions, for which the intricate phase diagram is mapped out in the case of a strong QP potential (equaling in strength the interparticle repulsion). In particular, making use of a generalized atomic-limit approach, the appearance of gaps in the many-body spectrum is quantitatively ascribed to quantum finite-size effects, due to the finiteness of the potential wells in the QP potential.

We have furthermore discussed the behavior of the system in a QP potential plus a parabolic trap, as required for a meaningful comparison to the experiments. The concept of a *local phase*, which is at the heart of the local-density approximation, applies successfully to a system without (pseudo)disordered potentials exhibiting homogeneous MI

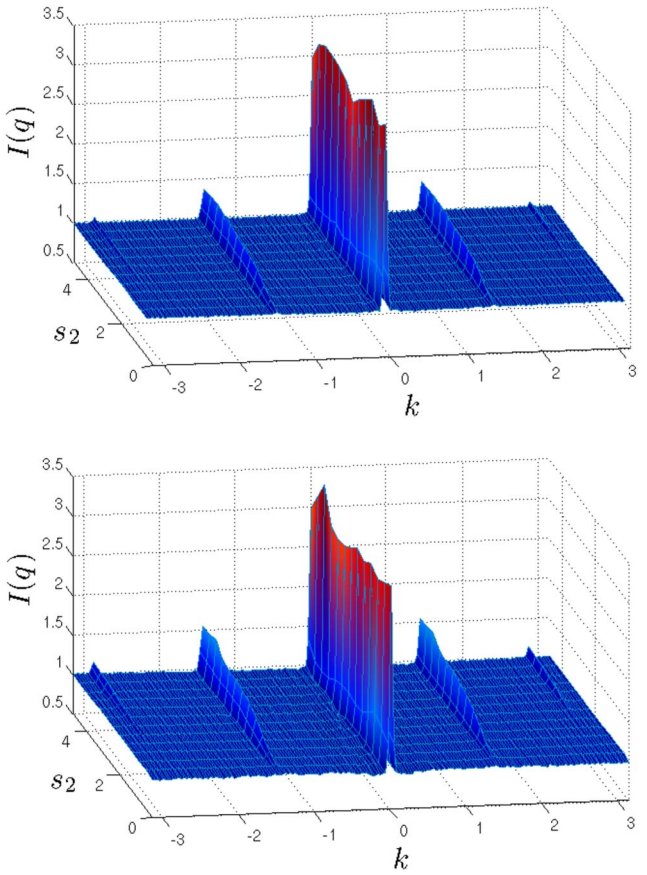

FIG. 29. (Color online) Upper panel: noise correlations for bosons in an incommensurate superlattice, same parameters as in Fig. 28 (upper panel). Lower panel: same quantity for the model, Eq. (24), *without* accounting for the hopping modulation.

and SF phases, but this concept fails to apply to the case of a BG, whose fundamental signature, a finite local compressibility, comes from localized gapless excitations which most likely do not appear in a single realization of the trapped system. A finite local compressibility can only be attained on average over the various local potential realizations (namely, over different spatial phase shifts). Nonetheless, the LDA picture for a local BG phase might be too restrictive; namely, nontrivial low-energy particle-hole excitations might appear in the trap which are not present in the bulk system, due to accidental quasidegeneracies of particle and hole states between different regions of the trap.

The above results show that the behavior of the Bose-Hubbard model in a QP potential is more complex than that of more widely investigated dirty-boson systems [4,5] and that in this respect a QP potential applied to the Bose-Hubbard model cannot be ascribed to the family of short-range correlated disorder potentials, given that correlations in such a potential are actually *long ranged*. Both at the single-particle level and at the many-body level a QP potential leads to a behavior which is intermediate between that of a system in a random potential and that in a commensurate periodic potential: indeed, the potential's spatial features, albeit aperiodic, have a definite upper bound in length scale, which introduces in turn a characteristic energy scale in the system. Such an energy scale shows up in the opening of gaps at incompressible regions of the phase diagram.

If a second QP potential at a different frequency is superimposed onto the first one, preliminary results show that the picture of a short-range correlated random potential is recovered, as the resulting physics of the Bose-Hubbard model in such a potential appears to mimic that of the same model in a truly random potential. In the presence of parabolic confinement, we have moreover shown that a two-color QP potential can realize a BG phase *all over the trap* on average over spatial phase fluctuations of the two potential components. Hence the gap between the single-color QP potential and an ideal (white-spectrum) random potential can be possibly bridged by enriching the QP potential with uniquely one more color. This conclusion has immediate practical consequences for the ongoing effort of realizing analog quantum simulators of correlated systems in a random environment within an optical-lattice setup, because the experimental requirement to bridge the gap between pseudodisorder and true disorder could be in practice the addition of one or a few extra laser standing waves.

A final, delicate aspect is the identification of an experimental signature for the occurrence of a BG insulating phase. This issue appears unresolved by the currently accessible observables—e.g., through time-of-flight measurements. This is intrinsically due to the fact that a BG is not characterized by correlations, which are generally akin to those of more conventional insulators, but by the spatial and energetic structure of excitations. A method to resolve the nature of these excitations, based on measuring the system's response upon variations of the trapping frequency, will be presented in a forthcoming publication [52].

ACKNOWLEDGMENTS

I would like to thank G.G. Batrouni, J.I. Cirac, and S. Wessel for useful exchanges and, particularly, L. Fallani, C. Fort, V. Guarrera, M. Inguscio, and J. Lye for enlightening discussions on the experimental subtleties. Part of the calculations presented in this work have been performed on the HPC cluster at the University of Southern California; I thank S. Haas for constant support. I would also like to thank the Institut "H. Poincaré" in Paris for hospitality within the program "Gaz Quantiques," during which part of this work was completed. This work is supported by the EU through the SCALA integrated project.

[1] D. J. Thouless, Phys. Rep., Phys. Lett. **13**, 93 (1974).
[2] B. Kramer and A. MacKinnon, Rep. Prog. Phys. **56**, 1469 (1993).
[3] D. K. K. Lee and J. M. F. Gunn, J. Phys.: Condens. Matter **2**, 7753 (1990).
[4] T. Giamarchi and H. J. Schulz, Europhys. Lett. **3**, 1287 (1987); T. Giamarchi and H. J. Schulz, Phys. Rev. B **37**, 325 (1988).
[5] M. P. A. Fisher, Peter B. Weichman, G. Grinstein, and D. S. Fisher, Phys. Rev. B **40**, 546 (1989).
[6] J. E. Lye, L. Fallani, M. Modugno, D. S. Wiersma, C. Fort, and M. Inguscio, Phys. Rev. Lett. **95**, 070401 (2005).
[7] D. Clément, A. F. Varón, M. Hugbart, J. A. Retter, P. Bouyer, L. Sanchez-Palencia, D. M. Gangardt, G. V. Shlyapnikov, and A. Aspect, Phys. Rev. Lett. **95**, 170409 (2005).
[8] C. Fort, L. Fallani, V. Guarrera, J. E. Lye, M. Modugno, D. S. Wiersma, and M. Inguscio, Phys. Rev. Lett. **95**, 170410 (2005).
[9] T. Schulte, S. Drenkelforth, J. Kruse, W. Ertmer, J. Arlt, K. Sacha, J. Zakrzewski, and M. Lewenstein, Phys. Rev. Lett. **95**, 170411 (2005).
[10] L. Fallani, J. E. Lye, V. Guarrera, C. Fort, and M. Inguscio, Phys. Rev. Lett. **98**, 130404 (2007).
[11] J. E. Lye, L. Fallani, C. Fort, V. Guarrera, M. Modugno, D. S. Wiersma, and M. Inguscio, Phys. Rev. A **75**, 061603(R) (2007).
[12] D. R. Hofstadter, Phys. Rev. B **14**, 2239 (1976).
[13] A. Aubry and C. André, in *Proceedings of the Israel Physical Society*, edited by C. G. Kuper (Adam Hilger, Bristol, 1979), Vol. 3.
[14] M. Kohmoto, L. P. Kadanoff, and C. Tang, Phys. Rev. Lett. **50**, 1870 (1983).
[15] S. Ostlund, R. Pandit, D. Rand, H. J. Schellnhuber, and E. D. Siggia, Phys. Rev. Lett. **50**, 1873 (1983).
[16] J. B. Sokoloff, Phys. Rep. **126**, 189 (1985).
[17] A. M. Rey, I. I. Satija, and C. W. Clark, Phys. Rev. A **73**, 063610 (2006); A. M. Rey, C. W. Clark, and I. I. Satija, Laser Phys. **17**, 205 (2007).
[18] V. W. Scarola and S. Das Sarma, Phys. Rev. A **73**, 041609(R) (2006).
[19] R. T. Scalettar, G. G. Batrouni, and G. T. Zimanyi, Phys. Rev. Lett. **66**, 3144 (1991).
[20] S. Rapsch, U. Schollwöck, and W. Zwerger, Europhys. Lett. **46**, 559 (1999).
[21] N. V. Prokof'ev and B. V. Svistunov, Phys. Rev. Lett. **80**, 4355 (1998).
[22] D. Jaksch, C. Bruder, J. I. Cirac, C. W. Gardiner, and P. Zoller, Phys. Rev. Lett. **81**, 3108 (1998).
[23] M. Greiner, O. Mandel, T. Esslinger, T. W. Hänsch, and I. Bloch, Nature (London) **415**, 39 (2002).
[24] T. Stöferle, H. Moritz, C. Schori, M. Köhl, and T. Esslinger, Phys. Rev. Lett. **92**, 130403 (2004).
[25] I. B. Spielman, W. D. Phillips, and J. V. Porto, Phys. Rev. Lett. **98**, 080404 (2007).
[26] B. Paredes, A. Widera, V. Murg, O. Mandel, S. Fölling, J. I. Cirac, G. V. Shlyapnikov, T. W. Hänsch, and I. Bloch, Nature (London) **429**, 277 (2004).
[27] E. Lieb, T. Schultz, and D. Mattis, Ann. Phys. **16**, 407 (1961).
[28] A. W. Sandvik, Phys. Rev. B **59**, R14157 (1999); O. F. Syljuåsen, Phys. Rev. E **67**, 046701 (2003).
[29] E. L. Pollock and D. M. Ceperley, Phys. Rev. B **36**, 8343 (1987).
[30] S. Wessel, F. Alet, M. Troyer, and G. G. Batrouni, Phys. Rev. A **70**, 053615 (2004).
[31] M. Rigol and A. Muramatsu, Phys. Rev. A **69**, 053612 (2004); Opt. Commun. **243**, 33 (2004).
[32] We note that the definition, Eq. (6), for the momentum distribution is strongly dependent on the considered size L in the case of a trapped system, where all the particles are confined in a finite region of space and L can far exceed this region. Throughout the paper we specify the size of the overall lattice used to host the trapped system, and in any case this size has always been chosen so as to be of the order of the trapped atomic cloud.
[33] V. G. Rousseau, D. P. Arovas, M. Rigol, F. Hébert, G. G. Batrouni, and R. T. Scalettar, Phys. Rev. B **73**, 174516 (2006).
[34] The change from periodic to antiperiodic boundary conditions can always be absorbed into the twist of π of a single bond in the Hamiltonian, as shown in Eq. (4).
[35] J. T. Edwards and D. J. Thouless, J. Phys. C **5**, 807 (1972).
[36] G. G. Batrouni, R. T. Scalettar, and G. T. Zimanyi, Phys. Rev. Lett. **65**, 1765 (1990).
[37] T. D. Kühner, S. R. White, and H. Monien, Phys. Rev. B **61**, 12474 (2000).
[38] We notice that the plateaus emerging from the QMC and random-atomic-limit calculation are also observed in the hard-core limit; see Fig. 1. Nonetheless, the width of the plateaus appears to be significantly reduced in the soft-core case (with $J/U=0.04$) with respect to the hard-core one for the same ratio of V_2/J.
[39] J. K. Freericks and H. Monien, Phys. Rev. B **53**, 2691 (1996).
[40] T. Roscilde, Phys. Rev. B **74**, 144418 (2006).
[41] S. Bergkvist, P. Henelius, and A. Rosengren, Phys. Rev. A **70**, 053601 (2004).
[42] C. Kollath, U. Schollwöck, J. von Delft, and W. Zwerger, Phys. Rev. A **69**, 031601(R) (2004).
[43] In fact, $\Delta E_{\mathrm{p-h}}$ overestimates in principle the interaction energy, because it contains the interaction of an extra particle with a background of N particles, instead of $N-1$ as in a system with fixed particle number N.
[44] In this respect it is worth noticing that, in the bulk system, low-energy particle-hole excitations can correspond to the transfer of a quasiparticle between two arbitrarily distant points. This is best understood in the classical limit $J\rightarrow 0$, where low-energy particle-hole excitations simply correspond to displacing a particle between two sites at quasidegenerate values of the local chemical potential. The periodicity of a truly incommensurate local chemical potential is by definition infinity, so that pairs of sites which are closest in energies can find themselves at opposite ends of the system. Nonetheless, other accidental, nonsystematic quasidegeneracies at shorter distances (from the quasiperiod up) can be expected, either associated with the external potential alone (possibly including the trapping one) or with the sum of the potential and of the interparticle interactions.
[45] L. Fallani (private communication).
[46] More quantitatively, a one-dimensional quasicondensate should behave as a Luttinger liquid, for which the coherent fraction $n(k=0)$ scales with the number of particles as $N^{1-K/2}$, where K is the Luttinger exponent; the well-known upper

bound [4] for K in a disordered potential, $K<2/3$, imposes that the coherent fraction cannot grow slower than $N^{2/3}$. Hence finding a coherent fraction $n(k=0)\ll N^{2/3}$ is a strong indication of the absence of quasicondensation. In the considered example, we have $\langle N\rangle\approx 127$, $\langle N\rangle^{2/3}\approx 25$, and $n(k=0)\approx 2.2$ (see Fig. 20).

[47] J. P. Grondalski, P. M. Alsing, and I. H. Deutsch, Opt. Express **5**, 249 (1999).

[48] E. Altman, E. Demler, and M. D. Lukin, Phys. Rev. A **70**, 013603 (2004).

[49] S. Fölling, F. Gerbier, A. Widera, O. Mandel, T. Gericke, and I. Bloch, Nature (London) **434**, 481 (2005).

[50] P. Buonsante and A. Vezzani, Phys. Rev. A **70**, 033608 (2004); P. Buonsante and A. Vezzani, *ibid.* **72**, 013614 (2005); R. Roth and K. Burnett, *ibid.* **68**, 023604 (2003).

[51] P. Sengupta, A. Raghavan, and S. Haas, New J. Phys. **9**, 103 (2007).

[52] T. Roscilde, arXiv:0804.2769.

[53] V. Guarrera, L. Fallani, J. E. Lye, C. Fort, and M. Inguscio, New J. Phys. **9**, 107 (2007).

[54] W. Zwerger, J. Opt. B: Quantum Semiclassical Opt. **5**, S9 (2003).